SUPPLEMENTAL MATERIAL

1. Expanded Results

Double reporter to permanently label cardiomyocytes activation of aurora kinase B in vivo in large animals

To track mitotic events *in vivo* in large animals, we developed a new reporter system based on the Aurora kinase B (AurKB) promoter region activation. AurKB is one of the central protein kinases that ensure the proper execution and fidelity of mitosis and is expressed only for a short time during the mitotic phase, localizing to the central spindle during anaphase and in the midbody during cytokinesis[23]. It has been considered as a putative marker for mitosis in several cell types, including cardiomyocytes[24-26]. A recent study demonstrated that AurKB correct positioning to the midbody in cardiomyocytes during mitosis is positively correlated with cytokinesis and that 70% of the neonatal cardiomyocytes that express AurKB undergo complete cytokinesis with correct midbody positioning[25]. To develop this reporter, we used the previously well-characterized 1.8kb promoter region of the human AurKB gene, which is highly conserved between species[27], and cloned it into a lentivirus to drive the expression of GFP protein (Supplemental Fig. 12a). We will refer to this reporter as the AurKB-GFP reporter throughout the manuscript. We generated and validated this reporter to detect mitotic events in proliferating cells, e.g., HEK293 cells (Supplemental Fig. 12a). Live cell imaging of hiPS-CMs overexpressing 4F over 96 h showed GFP expression during the M phase, which reaches the maximum intensity during cytokinesis; in contrast, there is no GFP expression observed in lacZ-treated cells (Supplemental movie 1&2). In line with a previous report[25], live imaging of hiPS-CMs treated with 4F indicated that 70% of the GFP expressing cells completed cytokinesis while the remaining 30% were stuck in mitosis without completing cytokinesis (Supplemental Fig. 12b and Supplemental movie 1&2). Fixation and Immunostaining demonstrated that 36 h post-infection with 4F, the GFP signal is co-localized with the AurKB protein expression at the midbody during mitosis (Supplemental Fig. 12c-d).

AurKB protein expression fades after two days post-infection; however, the GFP protein remained and marked those 20-30% of hiPS-CMs infected with 4F adenovirus, with a decline in the GFP signal after day 4 (Supplemental Fig. 12e-f). EDU nuclei labeling was observed in GFP-positive cells (Supplemental Fig. 12e), indicating the S-phase's completion before entering the M phase. After demonstrating the AurKB promoter region's ability to reliably indicate mitosis (100%) and cytokinesis (70%) events in cardiomyocytes through transient expression of GFP, we developed a permanent marker for mitosis to be used *in vivo*. To this end, we developed a double reporter system to track mitotic events *in vivo* based on the AurKB promoter described above. In this reporter system, we cloned a Lox-DsRed-Stop-Lox-GFP construct under CAG promoter in lentivirus; in another lentiviral construct, we cloned the Cre encoding protein sequence under the influence of the AurKB promoter (AurKB-Cre) (Supplemental Fig. 13a). Using this double reporter system, all infected cells will become DsRed positive; when mitosis occurs, Cre recombinase will be expressed and will cut out the DsRed-Stop sequence, turning these cardiomyocytes permanently into GFP positive cardiomyocytes. Therefore, the presence of green cells will be an indication of mitotic events. We first validated the color switch in normally proliferating cells (HEK293) (Supplemental Fig. 13b). Then, we further validated the efficiency of this reporter system in detecting mitotic events induced by 4F in hiPS-CMs (Supplemental Fig. 13c-d). This reporter system indicates the number of infected cells (total red- and green-labeled cells) and the number of mitotic events (green-labeled cells). Therefore, the quotient of green and red cardiomyocytes provides a quantification of mitotic cardiomyocytes.

2. Expanded discussion

Understanding the process of human cardiomyocyte proliferation and the reprogramming steps needed for the cardiomyocytes to complete the process is essential to advance the field of cardiac regeneration. Several efforts comparing proliferating fetal cardiomyocytes and adult cardiomyocytes have yielded a certain degree of understanding of the process[28]. However, the

highly variable nature of fetal and adult cardiomyocytes limits the ability to elucidate the reprogramming events during cell cycle. In the present study, we attempted to identify the essential reprogramming events associated with direct cell cycle induction by monitoring the same post-mitotic human cardiomyocytes during proliferation at a single-cell transcriptomic level. First, we found that sarcomeric disassembly is an essential step for cardiomyocytes during mitotic stage. This finding is consistent with the recent suggestion that proteins responsible for sarcomere assembly, e.g., ephrin-B1, are essential elements for the cell cycle blockade in adult cardiomyocytes[29]. In addition, other studies have shown that sarcomeric disassembly is associated with cardiomyocyte mitosis/cytokinesis through other approaches that induce cardiomyocyte proliferation, such as modulation of Yap/Hippo[30] or Meis1/Hoxb13[31] signaling pathways. Most recently, a study showed that troponin-T deletion in hiPS-CMs increased their ability to perform cytokinesis[32].

Furthermore, we demonstrated that proliferating cardiomyocytes shift their metabolism from energy production to biosynthesis[33]. This finding is consistent with the need for new building blocks for cell growth and division. Recent studies suggest that glycolysis[34, 35], glucose oxidation[36], succinate dehydrogenase[37], and the mevalonate pathway[38] influence myocyte proliferation; our results build upon these previous reports and support the idea that metabolic activity changes may be required for successful myocyte cell cycle progression. Interestingly, a recent study demonstrated that switching the metabolic substrate from fatty acids to glucose induces cardiomyocyte cell-cycle progression[36]. Considering that glucose is a primary biosynthetic substrate in cardiomyocytes[39], this supports our finding that the switch from catabolic to biosynthetic activities is essential for cell cycle progression in cardiomyocytes.

The advantage of these temporal single-cell RNAseq studies is that we reached a time resolution that enabled us to compare two subpopulations of cardiomyocytes, both of which received 4F for 48 hours; one subpopulation was delayed entering mitosis while the other subpopulation was in

mitosis. This comparison will impact the field of cardiac regeneration and has been long-awaited. This comparison was not possible before because there was no approach to induce cardiomyocyte regeneration that reached the achieved efficiency with the 4F (15% of the total cell population). Furthermore, direct induction of cell cycle is a clean approach to understand the mechanism of cardiomyocyte proliferation, unlike other approaches that have many off-target effects, e.g., manipulations of YAP[30], a developmental gene that induces dedifferentiation, and use of microRNAs[40], which have multiple off-target effects. The fact that the results are in line with previous assumptions in the field based on our developmental understanding of the heart gives more confidence in the validity of the findings. One of the prominent questions in the field is: why, using several approaches to induce the cell cycle in cardiomyocytes, e.g., 4F[41, 42], YAP[30, 43-45], CyclinA2[46-49], do only a certain subset of the cells respond despite the fact that these factors are expressed in all cells either using viral or *in vivo* transgenic approaches? Our single-cell RNAseq suggests that a specific starting population with higher energetic capacity is primed to respond to the induced cell cycle activation, consistent with the notion that biosynthesis is an energy-demanding process[50]. Interestingly, two recent studies using nuclear RNAseq and spatial RNAseq have suggested the existence of five distinct cardiomyocyte populations in healthy, injured, and regenerating mouse hearts and that some of these populations are proliferative while others respond to ischemia[51, 52]. Further studies are needed to fully characterize this primed subpopulation and understand the reason(s) of their decline in adult mouse hearts.

The insights we gained into the process of cardiomyocyte proliferation and the ability to define the 15% cardiomyocyte subpopulation that temporarily undergoes mitosis at 48 h (mitotic subpopulation) and track the reprogramming events in this subpopulation motivated us to perform the next translational steps: that is to provide a proof of concept for the efficacy of this approach in improving cardiac function in animal models of heart failure. Interestingly, a recent study showed that AAV-mediated expression of microRNA-199a in infarcted pig hearts initially

stimulates cardiac repair through induction of cardiomyocyte proliferation; however, subsequent persistent and uncontrolled expression of the microRNA resulted in sudden arrhythmic death of most of the treated pigs[40]. Our previous *in vitro* and *in vivo* results show that myocytes undergo only one round of division after transduction with cell cycle factors because the overexpression of the 4F in cardiomyocytes is self-limiting through proteasome-mediated degradation of the protein products[41]. These findings were confirmed in our bulk and single-cell RNAseq, as several of the genes that are involved in ubiquitination are upregulated at the 48h time point when comparing LacZ to 4F (Source data 2) and comparing cluster 4 (mitotic subpopulation) and 8 (quiescent subpopulation) (Source data 10). However, since ubiquitination GO terms are mostly in the upregulated gene list, which is overwhelmed with the cell cycle GO terms, they didn't come at the top of the list shown in the figures.

To perform more translational steps, we needed to transiently and specifically express 4F in cardiomyocytes to induce one cycle of proliferation and avoid any adverse effects in other tissues. Over the past decade, there have been significant advances in gene-therapy delivery approaches for transient gene expression using either ModRNA[53] or NIL[54]. Although the modified RNA approach is a promising virus-free delivery system for transient expression, its poor delivery and specificity to cardiomyocytes limit its applicability. Therefore, NIL was the tool of choice for our animal studies for transient expression with high infection efficiency, as reviewed in[55]. Our data show that a polycistronic TNNT2-4Fpolycictronic-NIL induces 4F expression only in cardiomyocytes both *in vitro* and *in vivo*. Furthermore, TNNT2-4Fpolycistronic-NIL induces proliferation markers in hiPS-CMs, cardiomyocyte cytokinesis *in vivo* in MADM mice and significantly improves cardiac function in both rat and pig models of heart failure caused by myocardial infarction. More importantly, the long-term follow-up for four months post-treatment revealed sustained improvement in cardiac function with no obvious toxicity observed in the animals, either in the heart or in other organs. Continuous induction of cardiomyocyte proliferation,

even though it was initially effective in improving cardiac function after myocardial infarction, leads to arrhythmias in the long run[40]. Therefore, the current work provides proof of concept that using transient gene therapy to directly induce cardiomyocyte proliferation is effective and not toxic. This notion could be applied to other approaches that induce cardiomyocyte proliferation as well as other diseases. The carriers for transient gene therapy, which include NIL, modRNA, or direct protein delivery, could be targeted for specific tissues or cell subtypes. It is important to note that the *in vivo* effect might be, in part, a paracrine effect from the infected but not proliferating cells. This was evident in a recent study using hiPS-CMs overexpressing cyclinD2 and injected in pig hearts, which showed enhancement in cardiac function in part due to secretion of protective micro RNAs[56]. Even though we did not observe any major differences in gene expression between the quiescent populations that received the 4F and the lacZ, but this does not exclude potential differences in their secretome, which should be investigated in further studies.

We assessed the functional efficacy of the TNNT2-4Fpolycictronic-NIL over 16 weeks following injection in a subacute heart failure model where the virus was injected one-week post-I/R. A study of the safety and functional efficacy of the TNNT2-4Fpolycystronic-NIL in a more chronic setting of heart failure, where the treatment starts 4-8 weeks post-I/R, will be considered in the future to assess the appropriateness of this approach in the treatment of chronic heart failure. Theoretically, the advantage of inducing cardiomyocyte proliferation in the subacute phase of MI is that surviving cardiomyocytes are still relatively healthy and thus able to produce healthy daughter cells. Waiting for longer times until left ventricular dilatation and cardiomyocyte remodeling may hinder cardiomyocyte proliferation because mechanical stretch and oxidative stress impair cardiomyocyte function; at this stage, other therapeutic approaches such as direct cardiac reprogramming[57] to target the fibroblast pool may be more efficacious.

In conclusion, we have provided a mechanistic understanding of the process of forced cardiomyocyte proliferation and advanced the clinical feasibility of the 4F gene therapy approach

for subacute heart failure treatment by minimizing the oncogenic potential of the cell cycle factors with the use of a novel transient and cardiomyocyte-specific viral construct. Further studies are needed to prove effectiveness and safety over a longer period of time in heart failure models in large animals. These studies will pave the way for the first test of this promising approach in patients with ischemic cardiomyopathy.

Limitations of the study

The use of 60-day mature hiPS-CMs instead of adult primary human cardiomyocytes in the mechanistic studies is a limitation. However, there is a lack of a reliable long-term culture model of adult human cardiomyocytes and the inability to perform single-cell RNAseq on adult cardiomyocytes other than single nuclear RNAseq due to the large size of the adult cardiomyocytes. More importantly, nuclei are at different integrities during the cell cycle stages, which will lead to difficulties in isolating mitotic nuclei and will obfuscate the interpretation of any nuclear RNAseq. Therefore, we used the hiPS-CMs, which are highly pure cardiomyocyte cultures obtained from Cellular Dynamics, Inc. These cells are selected after differentiation using an α-MHC-Blastocidin selection cassette. This strategy yields nearly 100% pure iPSC-CMs, as evident in our TNNT2 immunostaining images and single-cell RNAseq data. For consistency, only cells that mature for at least 60 days were used for experiments. After this time, the cells have matured to a point at which they have minimal proliferation capacity and minimal basal expression of cyclins and Cdks[41] (Fig. 3c). Thus, the use of hiPS-CMs provided a homogenous cell population as a starting material to track the reprogramming events during cardiomyocyte proliferation. Furthermore, we validated the findings of cell cycle reprogramming from the hiPS-CMs in P7 neonatal cardiomyocytes.

The findings regarding the existence of a specific cardiomyocyte population that can respond to cell cycle induction are interesting. However, CD36 is not the only effector in this primed population. It is likely that there is a combinatorial effect of several factors that prime the

cardiomyocytes to enter the cell cycle. In line with this observation, a recent study has pointed out the existence of a primary proliferative population in mouse hearts that significantly declines but does not disappear up to 11 days after birth[51]. Another follow-up study has shown that this proliferative population of cardiomyocytes becomes enriched in the scar area after ischemia[52]. Furthermore, another recent study generated a Ki67 reporter mouse which demonstrated that there is a small sub-population of adult cardiomyocytes that can activate the cell cycle after ischemia and that the deletion of this subpopulation results in worsened outcomes after ischemia[58]. All these studies and our findings suggest the presence of different subpopulations of cardiomyocytes that respond differently to ischemia and cell cycle induction. Further studies are needed to fully characterize these subpopulations in adult mammalian hearts. As single-cell sequencing technologies with the spatial resolution are progressing and evolving, it seems likely that we will reach the ultimate aim of understanding the different types of cardiomyocytes within the adult human myocardium.

The AurKB reporter data must be interpreted cautiously as mitotic rather than cytokinetic events. As we described here, This reporter overestimates cytokinesis events by 30%. Nevertheless, as we show here, the reporter reliably estimates cell cycle induction and mitotic entrance in cardiomyocytes *in vitro*, *in situ,* and *in vivo* in large animal models with almost no background labeling in the control groups. We chose to use the CAG promoter for this reporter rather than TNNT2 due to the delayed kinetics of the TNNT2 promoter (Supplemental Fig. 7b-c), which could complicate the experimental design and interpretation of results.

3. Supplemental Methods

Cloning and preparation of integrating and non-integrating lentivirus.

cDNA of CAG promoter, TNNT2 promoter, Cre recombinase, AurKB promoter, CCNB, CCND, CDK1, and CDK4 were cloned into the pLenti-MCS-SV-puro backbone (Addgene). To produce the Lentivirus particles, $5X10^6$ HEK293 cells were transfected using FuGENE HD transfection

reagent (Promega) along with 5µg pMD2.g, 5µg psPAX2 (Integrating lentivirus) or psPAX2-D64V (non-integrating Lentivirus) (Addgene) and 10µg of the expression pLenti vector encoding the gene of interest for 48 h. The media containing the virus were collected and filtered through a Nalgene syringe filter 0.45 µm. For in vitro experiments, the virus was mixed with a polybrene transfecting reagent (1µg/ml) (Millipore Cat# 1003). The virus was then used to treat 60 days old hiPS-CMs (100 TU/cell). For *in vivo* injections, the virus solution was centrifuged at 20,000xg at 4°C for 2 h, and the pellet was resuspended in PBS. Modified RNA was synthesized and purchased from Bio-Synthesis, Inc. RNA modifications, transfection reagents, and procedures were conducted following the protocol described in[59].

Preparation and maintenance of hiPS-CMs

The human-induced pluripotent stem cell-derived cardiomyocytes (hiPS-CMs) were purchased from Cellular Dynamics (Currently FujiFilm Inc.). These hiPS-CMs have been selected after differentiation using an α-MHC-Blastocidin selection cassette. This strategy yields nearly 100% pure hiPS-CMs. hiPS-CMs were re-plated on fibronectin-coated plates and cultured in R.P.M.I. medium with a B27 supplement. Then the cardiomyocytes were maintained in RPMI/B27 supplement with insulin for 2–3 months.

Preparation of P7 neonatal cardiomyocytes

Primary mouse cardiomyocytes were isolated from 7-day-old C57/Bl6 mouse or CD36KO mice. The CD36KO mice were obtained from the Jackson Laboratory (JAX labs, B6.129S1-Cd36tm1Mfe/J Stock # 019006). The P7 neonatal cardiomyocytes were isolated by the established protocol described in [41, 60]. Briefly, neonatal pups were sacrificed, and neonatal hearts were isolated. The ventricles tissue was chopped into small pieces, and was digested by several rounds of 7-minute incubations in ADS buffer (0.68% NaCl (w/v), 0.476% HEPES (w/v), 0.012% NaH2PO4 (w/v), 0.1% glucose (w/v), 0.04% KCl (w/v), 0.01% MgSO4 (w/v), pH 7.35) containing 0.3 mg/ml collagenase A (Roche) and 0.6 mg/ml pancreatin (Sigma-Aldrich) at 37°C with continuous shaking. 3ml of Fetus bovine serum (FBS, Invitrogen) to each Digestions. All the

digestion was pooled together, and cells were centrifuged and resuspended in a plating medium (68% DMEM, 17% medium 199, 10% horse serum, 5% FBS) (Invitrogen). Cardiomyocytes were separated from non-cardiomyocyte cells by plating the mixture on tissue culture plates for 1h at 37^{o}C in 5% CO2. The suspended cardiomyocytes were then plated on laminin-coated tissue culture plates and incubated overnight at 37^{o}C in 5% CO2 to allow cellular attachment. The following day, cells were washed with PBS, and the plating medium was replaced with maintenance medium (79.5% DMEM, 19.5% medium 199, 1% FBS) supplemented with 1% Antibiotic-Antimycotic (Invitrogen).

siRNA Transfection

A mixture of 0.5µg of SiCD36 or Si control (Qiagen, SI00001330, SI03650318) lipofectamine RNAiMAX transfecting agent (Invitrogen cat # 13778-150), and OptiMEM media (Invitrogen 31985-070) was incubated at room temperature for 30 minutes to allow the DNA/RNA-liposome complexes to form. Next, OptiMEM/Lipofectectamine transfection mixture was added to the hiPS-CMs and incubated for 24h at 37^{o}C and 5% CO2. Then the cells were transfected with 4F or LacZ adenovirus for 48 h and then prepared for immunostaining or RT-PCR.

Bulk RNAseq analysis

RNA from hiPS-CMs or P7 neonatal cardiomyocytes were isolated using the Qiagen, miRNeasy Micro Kit, #210874, following homogenization of the tissue in QIAzol (Qiagen). Using the Ovation RNA-seq System v2 Kit (NuGEN), total RNA (20–50 ng) was reverse transcribed to synthesize the first-strand cDNA using a combination of random hexamers and a poly-T chimeric primer. The RNA template was then partially degraded by heating, and the second-strand cDNA was synthesized using DNA polymerase. Double-stranded DNA was then amplified using single primer isothermal amplification (SPIA). Random hexamers were then used to amplify the second-strand cDNA linearly. cDNA samples were fragmented to an average size of 200 bp using the Covaris S2 sonicator. Libraries were made from the fragmented cDNA using the Ovation Ultralow V2 kit (NuGen).

Following end-repair and ligation, the libraries were PCR amplified with 9 cycles. A Bioanalyzer assessed library quality on High-Sensitivity DNA chips (Agilent), and concentration was quantified by qPCR (KAPA). The libraries were sequenced on a Novaseq sequencer with a single-read, 50-cycle sequencing run (Illumina). We utilized the RNAseq-analysis pipeline reported previously[57]. For the readers' convenience and completeness of the current manuscript, we review the pipeline's critical steps/features and statistics below. Available adapters and low-quality regions of reads were trimmed using Fastq-mcf (http://code.google.com/p/ea-utils). Sample QC was assessed using FastQC (http://www.bioinformatics.babraham.ac.uk/projects/fastqc/). Reads were aligned to the GRCh38 genome using Tophat 2.0.13. Gene expression was tallied by Subread feature Counts using Ensemble's gene annotation for GRCh38 (human) and mm10 (mouse) genomes. Finally, we calculated differential expression P-values using edgeR 8. Here, we first filtered out any genes without at least two samples with a CPM (counts per million) between 0.5 and 5000. CPMs below 0.5 indicate nondetectable gene expression, and CPMs above 5000 are typically only seen in mitochondrial genes. If these high-expression genes were not excluded, their counts would disproportionately affect the normalization. After excluding these genes, we renormalized the remaining ones using "calcNormFactor" in edgeR, then calculated P-values for each gene with differential expression between samples using edgeR's assumed negative–binomial distribution of gene expression. Next, we calculated the false discovery rates (FDRs) for each P-value with the Benjamini-Hochberg method based on the built-in R function "p.adjust.". The genes that showed a fold change of 2 or more with significance of p_{adj} <0.05 are identified as the differentially expression genes between the groups. The Database for Annotation, Visualization and Integrated Discovery (DAVID) v6.8 was used for the GO term enrichment analysis (https://david.ncifcrf.gov/).

Contractile function monitoring of hiPS-CMs using CardioExcyte 96 system

hiPS-CMs were plated on fibronectin-coated NSP-96, CardioExcyte 96 Sensor Plates with extra stimulation electrodes. The NSP-96 plate was maintained in the CardioExcyte 96 system at 37˚C

and 5% CO_2. The cells were electrically stimulated at 1Hz during the experiments. Impedance recordings were performed every 30 minutes for 96 h. The data were analyzed with CardioExcyte 96 analysis software.

Electrophysiological recordings of the ionic current of hiPS-CMs

Sodium current (I_{Na}) was recorded in the whole-cell configuration of the patch-clamp technique. All recordings were performed at room temperature (20° to 22° C). The pipette solution consisted of (in mmol/L): 120 KCl, 1 $MgCl_2$, 3MgATP, 10 Hepes, 10 EGTA, pH 7.3. Bath solution contained (in mmol/L) 140 NaCl, 5.4 KCl, 1.2 KH_2PO4, 5 HEPES, 5.55 glucose, 1 $MgCl_2$, 1.8 $CaCl_2$, pH 7.4. R_{series} was compensated >80%; no corrections were made for liquid junction potentials. Data were analyzed with either Clampfit 11 (Molecular Devices) or Igor, dPatch/SutterPatch (Sutter Instruments).

Single-Cell RNA-Sequencing Library Generation

hiPS-CMs either infected with LacZ or 4F for the indicated time were filtered using a 70μM filter, resuspended in 1% B.S.A. in PBS, and counted immediately before library preparation. G.E.M. Generation and Barcoding were performed following the Chromium Single Cell" Reagents Kits v3 Rev A User Guide with Chromium Single Cell" G.E.M., Library and Gel Bead Kit v3 (10X Cat # 1000092). Briefly, the Chromium chip was loaded, and the Chromium Single Cell B program was selected. The chip was ejected immediately following the completion of the program. 100 μL of recovered G.E.M.s was slowly pipetted and transferred to tubes precooled on ice. The G.E.M.s were then incubated for the R.T. reaction using a thermal cycler at 53˚C for 45 min, then 85˚C for 5 min, followed by a 4˚C hold. Samples were then stored at -20˚C overnight. All libraries were pooled and sequenced using the NovaSeq to a read depth of at least 50,000 reads per cell. The sequenced reads for each sample were mapped to the GRCh38 genome to generate the (gene-by-cell) count matrix using cell ranger count (Cell Ranger version 3.1.0 from 10x Genomics) with default parameters. The counts" matrices across the samples were aggregated using cell ranger aggr. The resulting files were processed in R using the package Seurat (version 3.1.3)[61]. All cells

with at least three detected genes and less than 30% of reads from mitochondrial genes and all detected genes in at least 200 cells were used in the further analyses. The remaining data were normalized using the "LogNormaliz" method. Principal Component Analysis for the subset of the 2000 most variable genes (Seurat function FindVariableFeatures) was then performed on the scaled data. The cells were clustered using the Louvain Algorithm with the resolution parameter value of 0.5 (Seurat function FindClusters) after determining the shared nearest neighbor graph using the first ten principal components (Seurat function FindNeighbors). The data were visualized using the UMAP algorithm with the first ten principal components as input (Seurat function RunUMAP). The cells were grouped into ten clusters based on the distribution of expression of the cell cycle genes of interest. Differential analysis between all pairs of clusters was performed using the Wilcoxon rank-sum test to identify the differentially expressed genes (Seurat function FindMarkers). The dimensionality reduction results were reformatted for compatibility with the learn_graph function in the R package monocle3, and scmap used for trajectory analysis[62, 63]. This analysis was done for clusters 1-9. According to the developer of MONOCLE the limitations for pseudo time trajectory are that “Monocle doesn't know a priori which of the trajectory of the tree to call the "beginning"” and “if you don't have a timeseries, you might need to set the root based on where certain marker genes are expressed, using your biological knowledge of the system." (http://cole-trapnell-lab.github.io/monocle-release/docs/). However, as we already know the time series order (24 h to 72 h) and the cell cycle marker gene expression (pre-mitotic to mitotic) we were able to perform the MONOCLE pseudo time trajectory analysis avoiding these limitations.

Immunocytochemistry and immunohistochemistry

The hiPS-CMs or P7 neonatal cardiomyocytes were fixed in 4% formaldehyde for 20 min (Thermos Scientific Cat#28908). Fixed cells were washed three times with PBS. For animal experiments, the heart was isolated and perfused with 1M KCL to arrest the heart, then washed with PBS and perfused with 4% paraformaldehyde (Electron microscopy sciences Cat# 15713-

S). The hearts were cut longitudinally into half and kept in 4% paraformaldehyde for 48 h. The hearts were then washed with PBS, then placed in 10% sucrose solution for 1 h followed by 20% sucrose solution for 1 h at room temperature, then placed in 30% sucrose solution overnight at 4^{o}C. The hearts were then processed into frozen OCT blocks and kept at -80^{o}C for 24 h. Next, the heart was sectioned using a cryostat (Leica Inc.) in 8µm thick sections, placed on slides, and kept at -20^{o}C until staining. To start staining, the OCT was removed from the section by heating at 95^{o}C for 5 min then washing in PBS for 30 min.

The fixed cells or cleaned sections were permeabilized with 0.1% Triton X-100 for 15 min (Millipore Cat# 55163804) and then blocked with 3% bovine serum albumin (B.S.A.) in PBS for 60 min at room temperature (V.W.R. Cat# 0332). The cells or tissue sections were then probed with primary antibody (1:200 in 1% B.S.A.) for 1.5 h. Then washed three times with PBS. They were then labeled with secondary fluorescent antibody (1:200 in 1% B.S.A.). Tables 1&2 showed a list of primary and secondary antibodies used in this study. Cells/ tissue sections were then washed three times with PBS and stained with DAPI 1µg/ml (Biotium Cat# 40043) to stain the nucleolus blue. For EDU detection, the cells were also treated with 5µM 5-ethyl-2-deoxyuridine (EDU) for the course of the experiment, which will incorporate into the newly synthesized DNA. After fixation, permeabilization, and blocking of the cells/ tissue sections, the EDU incorporation was visualized using the Click it EDU-Alexa-Flour^{647} imaging kit (Thermo Fisher Cat# C10340). The cells were treated with NucBlue live cells stain (Thermo Fisher) for 20 minutes for live-cell imaging. For the cross-sectional cell size staining, the cleaned sections were incubated with 5ug/ml Wheat Germ Agglutinin (WGA , Thermofischer W32464) for 30 min. and then stained with DAPI 1µg/ml. The slides were incubated with Sudan Black (1mg/ml) for 30 min to reduce the background.

Imaging was conducted for the whole well or heart section using the high content imaging instrument, Cytation 1. The percentage of co-localization of PHH3, EDU, GFP, or gene expression

and Troponin-T was quantified using Gen 5.05 software. Cell size was measure using image J software.

Immunoblotting: The hiPS-CMs or heart tissue were lysed in RIPA lysis buffer (VWR, N653) plus 1% Halt™ Protease and Phosphatase Inhibitor Cocktail (Thermofisher scientific, 78440). The protein was denatured at 95° C for 5 minutes, separated by 4-12% Bis-Tris gel (Invitrogen, NW64120), and electrophoretically transferred onto nitrocellulose membranes (Invitrogen). Membranes were then washed in TBST, blocked with 3%BSA, and then incubated with primary antibodies at 4oC overnight. The primary antibodies listed table 1 below were used in concentration 1:1000 in 1% BSA). Next, membranes were washed in TBST and labeled with secondary antibody (1:2500 in 1% BSA). The blots were then stripped with stripping buffer (Thermos scientific, 46428) for 15 min at RT. The blots were then probed with Recombinant HRP Anti-GAPDH antibody [EPR16891] (Abcam, ab201822). The image was captured by the ChemiDoc imaging system and analyzed with ImageJ software.

Table 1: Primary Antibodies

Specific protein	**Primary antibody**	**Cat #**
Cardiac Troponin	Mouse Monoclonal Cardiac Troponin T Antibody	Thermos Fisher (MA5-12960)
Cardiac troponin	Rabbit monoclonal Anti-Cardiac Troponin T antibody	Abcam ab209813
Phospho Histon H3 (PHH3)	Rabbit monoclonal Anti-Histone H3 (phospho S10) antibody - ChIP Grade	Abcam ab5176
CDK4	Rabbit monoclonal Anti-CDK4	Abcam ab199728
CCNB	Rabbit monoclonal Anti-CCNB	Abcam ab32053
CCND	Rabbit monoclonal Anti-CCND	Abcam ab134175
CDK1	Mouse monoclonal Anti-CDK1	Abcam ab18

Arura Kinase B	Rabbit polyclonal anti-Aurora B	Abcam ab2254
Ds Red	Mouse monoclonal anti R.F.P.	Abcam ab150115
CD36	APC Anti-CD36 antibody [TR9]	Abcam ab82405

Table 2: Secondary Antibodies

Secondary antibody	**Cat #**
Goat anti-Mouse IgG (H+L), F.I.T.C.	Thermos fisher A16079
Texas Red Goat anti-Rabbit IgG (H+L)	Thermos fisher T-6391
Alexa Flour™ 647 donkey anti-rabbit IgG	Thermos fisher A31573
Texas Red -X goat anti-mouse IgG	Thermos fisher T862
Anti-GFP, rabbit polyclonal antibody Alexa Fluor™ 448 conjugate	Thermos fisher A21311
Peroxidase-conjugated Donkey anti-Mouse IgG(H+L).	Jackson immuneResearch, 715-035-150
Peroxidase-conjugated Goat anti-Rabbit IgG(H+L).	Jackson immuneResearch, 111-035-144

qRT-PCR

A piece of the left ventricle at the injection area was collected for RNA extraction. The heart was homogenized with QIAzol lysis reagent (Qiagen Cat# 79306), or hiPS-CMs cells plated in 24 well plates were washed with PBS then treated with QIAzol lysis reagent. RNA was extracted following the miRNeasy micro kit protocol (Qiagen Cat# 217084). The concentration of the RNA was calculated using the Cytation 1 reader. 1ug of each RNA sample was used for reverse transcription using a mixture of oligo(dT) and random hexamer primers (SuperScript IV VILO Master Mix, ThermoFisher Scientific Cat # 11756050). Real-time PCR analysis was conducted with Taqman fast advanced master mix (Thermo Fisher 4444557), and primers specific to human CDK1, CDK4, CCNB, CCND, CD36 genes (Hs00938777, Hs00364847, Hs01030099,

Hs00765553, Hs00354519 respectively, Applied Biosystem), and the expression was normalized to rat GAPDH expression (Rn01775763, Applied Biosystem) or human GAPDH expression for hiPS-CMs (Hs02786624, Applied biosystem) using the Quant studio 5 real-time PCR detection system (Applied Biosystems).

Animal experiments

Animal studies were performed following the University of Louisville animal use guidelines, and the protocols were approved by the Institutional Animal Care and Use Committee (IACUC) and were accredited by the Association for Assessment and Accreditation of Laboratory Animal Care.

MADM mice experiment

For lineage tracing, we used mosaic analysis with double markers (MADM) transgenic mice were developed as prescribed in [41]. All the surgeries were performed as described in [64, 65]. Adult (about 12 weeks old) female MADM mice were anesthetized with sodium pentobarbital (60 mg/kg i.p.). After opening the chest through a left thoracotomy, a nontraumatic balloon occluder was implanted around the mid-left anterior descending coronary artery (L.A.D.) using an 8-0 nylon suture. Myocardial infarction was produced by 60-min coronary ischemia, followed by reperfusion (I/R). Rectal temperature was carefully monitored and maintained around 37°C throughout the experiment. Successful performance of coronary occlusion and reperfusion was verified by visual inspection and by observing S-T segment elevation and widening of the QRS on the electrocardiogram during ischemia and their resolution after reperfusion. Seven days after I/R, mice were re-anesthetized with sodium pentobarbital, 60 mg/kg I.P. and the chest reopened through a central thoracotomy. The mice were randomly selected to be injected with 20 ul of TNNT2-4Fpolycistronic-NIL, LacZ-NIL virus intramyocardially using a 30-gauge needle. The injections were made at the border between infarcted and non-infarcted myocardium as two injections 10 µL each ($2x10^7$ transducing units (TU) per mouse heart). Forty-eight hours after injection, mice received Tamoxifen (40mg/kg I.P.) for three days (Sigma Aldrich T5648). Mice

were euthanized 14 days after MI, and the hearts were harvested for pathology study. The mice sergeant was blinded to all administered viruses.

MADM mice frozen hearts were sectioned Longitudinally into 180-210 sections (3 sections per slide collect one and throw away 2) 8μm thick. The frozen sections were fixed, permeabilized, and blocked as described in Immunocytochemistry and immunohistochemistry section, then stained with Dapi 1μg/ml (Biotium Cat# 40043) to stain the nucleolus blue. The Coverslips were mounted with Vectashield antifading medium (vector labs Cat# H-1000) onto slides and visualized using Keyence BZ9000 imaging system (10X magnification to the whole left ventricle). The percentage of single-colored cardiomyocytes from the total labeled cardiomyocytes was calculated using B.Z. Analyzer software. Individuals who analyzed the results were blinded to the treatment applied in each animal.

Rat experiments

All surgeries were performed as described in [66, 67]. Briefly, Female Fischer 344 (F344) rats at the age ranging from 8-12 weeks were anesthetized with ketamine (37 mg/kg) and xylazine (5 mg/kg), intubated, and ventilated with a rodent respirator. Anesthesia was maintained with 1% isoflurane inhalation, and body temperature was kept at 37°C with a heating pad. All rats underwent a 2 h occlusion of the left anterior descending coronary artery, followed by reperfusion. Seven days after MI, echocardiography was performed to ensure the development of MI. All rats in this study had EF drop > 20 points from baseline. Rats were randomized into two groups (Control-NIL, TNNT2-4F-NIL). Rats were re-anesthetized with ketamine/xylazine, intubated, and ventilated. The chest was reopened to expose the heart. Viral vectors ($1x10^8$ TU per rat heart in 100 μl PBS) were injected into the left ventricle along the infarct border at five sites (20 μl/site) using a 30G needle. The rat surgeon was blinded to whether 4F or control non-integrated lentivirus was administered in each animal.

Cardiac function was assessed by serial echocardiography at baseline (before MI), one week after MI (before virus injection), and then every four weeks after virus injection. Animals were

anesthetized lightly with isoflurane, placed on the imaging table in the supine position, and prepared for imaging using the Vevo 2100 Imaging System (Visual Sonics) equipped with a 25-MHz transducer. Parasternal longitudinal axis images were acquired and analyzed by LV trace using the Vevo LAB 3.2.6 to obtain the LV functional parameters, including the end-diastolic and end-systolic area, volume, stroke volume, fractional shortening, and ejection fraction. Imaging and calculations were done by an individual who was blinded to the treatment, and the code was broken after all data was acquired.

At the end of the experiments (5 or 17 weeks after MI), animals were sacrificed, and their hearts were harvested for histological studies. The frozen hearts were sectioned longitudinally into 400-500 sections 8um thickness (take a section to throw one add two sections per slide), and one slide for every ten slides (20-25 slide per animal) were stained with Standard Masson's Trichrome staining to determine scar size. The stained sections were imaged using the Keyence BZ9000 imaging system (4X magnification). Image J software was used to measure the scar area (blue) and healthy area (red) on longitudinal sections. Individuals assessing scar area were blinded to the treatment applied in each animal.

Four slides per heart were stained with WGA. Image J software was used to measure the cross-sectional cell size of 140-150 cells per animal at the border zone or the remote zone.

Pig experiments

All surgeries were performed as described in[68]. Three months old Yorkshire pigs weighing 25-35 kg received 200 mg amiodarone orally daily for seven days pre-operatively. Pigs were premedicated with an intramuscular injection of a solution containing ketamine hydrochloride and xylazine.

Pigs were injected with a dose of buprenorphine S.R. before the procedure. To create myocardial infarction, the right neck's skin was cut to make a small opening, allowing access to the right carotid artery. A 7-8F fast-cath sheath was introduced into the carotid artery. The pig was injected with Heparin (300 units/kg I.V.) to prevent clotting of the sheaths and catheters during the

procedure. After intubation, the pig was mechanically ventilated. Anesthesia was maintained with isoflurane. Body temperature was monitored continuously with a rectal probe attached to a thermocouple and maintained within physiology range using a veterinary blanket. The pigs were subjected to 5 minutes of stabilization, followed by baseline echocardiography.

A 6-7F Hockey-stick catheter was guided to the left main coronary artery under fluoroscopy as following: the catheter engaged the left main coronary ostium, and an angioplasty-type balloon catheter and guidewire assembly were fluoroscopically guided into the LAD. Then, the wire was advanced into the distal LAD, and an appropriate balloon catheter was telescoped over the wire and positioned above the first diagonal branch (the entire LAD territory was included for occlusion). The balloon's placement will be verified by intracoronary contrast dye injection (Contrast media) and documented by cine angiogram before inflation. The balloon was inflated to occlude the LAD, and the LAD occlusion was maintained for 90 minutes to produce myocardial infarction, targeting an infarct size of >50% of the area at risk. Inflation and position of the balloon were verified by contrast angiogram again at the end of ischemia. If necessary, the balloon will be repositioned, and such "positional re-inflation" will be limited to less than 20 seconds to avoid any preconditioning. Once the balloon is inflated, external defibrillator pads were placed on the pig's chest for "hands-free" cardioversion if ventricular fibrillation occurs using a bipolar defibrillator (HP Codemaster XL+) at 300 Joules. After the 90 min ischemic period, the intracoronary balloon was deflated to initiate reperfusion. After the procedure of myocardial infarction, the balloon catheter was withdrawn, and a cine angiogram was taken to document the wide open of the L.A.D. artery. After withdrawing the Hockey-stick guide catheter, the arterial sheath catheter was removed, and the arterial was repaired by anastomosis. The skin incision was closed in 3 layers using 3-0 Vicryl for internal sutures and 3-0 P.D.S. for the final subcutaneous layer. The pig was weaned from anesthesia, and the animal was extubated when appropriate and allowed to recover. Animals received antimicrobial therapy cetiofur pre-operatively and every 24 hours for the first 48 hours postoperatively. Animals were prepped and

draped in a routine sterile fashion. 5% dextrose and normal saline was continuously infused during the procedures

Seven days after the MI procedure, pigs were re-anesthetized as described above. Pigs were subjected to MRI scans and echocardiography. Anesthesia was maintained with isoflurane. Body temperature was monitored continuously with a rectal probe attached to a thermocouple and maintained within physiology range using a veterinary blanket. Animals will be prepped and draped in a routine sterile fashion. A dose of buprenorphine S.R. will be given before the procedure. The chest was opened through the initial skin incision and continued down to the sternum. To avoid a post-surgical pulmonary complication, a midline sternotomy to expose the heart in the intrapleural space without breaking the pleural membrane was performed with extra care to avoid rapture of the pleural membrane intact during the opening of the mediastinum. Then the heart is suspended in a pericardial cradle as described in [69, 70].

In the case of the pleural membrane broken, efforts are made to close the tear by re-approximation of the pleural membrane with 6-0 Prolene and to reestablish a negative pressure in the pleural cavity using a withdrawal tube with a purse-string closure. After the chest was opened, the pericardium was cut vertically, and the heart was exposed and suspended in a pericardial cradle. Five intramyocardial injections (200μl each) ($1.5X10^9$ TNNT2-4F-NIL or lacZ-NIL plus $1.5X10^9$ Double reporter. Total $3x10^9$ TU total/pig heart) of viral vectors were performed along the infarct border, and the site of injection was demarcated with a 6-0 Prolene suture. After completing these procedures, warm normal saline (approx. 500mL) was used for flushing the thoracic cavity. This flush was suctioned out before closing the chest. The pericardium was approximated as soon as possible. The sternum was closed with a 20G stainless steel suture and 5 Green Braided P.T.F.E. nonabsorbable surgical sutures. The chest was closed in layers (0 PDS II suture for the muscle and 2-0 PDS II suture subcutaneously), and a single mediastinal tube (18F catheter), 3-way valve, and 60cc syringe will be used to reestablish a negative intrapleural pressure and evacuate any remaining blood or irrigation solution. The chest tube (18F catheter)

was removed before skin closing after no visible air leak or blood accumulation, and a purse-string suture (2-0 PDS II) was used to ensure an airtight seal. The skin incision was then glued with Vetbond adhesive. Then the chest was closed, and the inhaled anesthetic was turned off, the animal extubated when appropriate, and allowed to recover. Animals received antimicrobial therapy cetiofur pre-operatively and every 24 h for the first 48 h postoperatively.

Four weeks after virus injection animal was anesthetized with isoflurane as described before to perform the final cardiac MRI and echocardiography. Body temperature will be monitored and maintained within the physiological range. Arterial blood pressure and surface E.C.G. were monitored continuously. Then the animal was deeply anesthetized with 5% isoflurane. A bolus of 3-6 ml/kg of 3M KCl solution will be injected into the left atrium until the heart is arrested. After the cessation of vital signs, the heart will be harvested for postmortem procession.

T.T.C. stain of the pig heart

Directly after the heart was harvested, the aorta was perfused with normal saline (500-1000 ml) to flush out vascular blood. The heart was weighed and transversely sliced into 5-6 sections. Heart sections were incubated in 1% T.T.C. at 37^{o}C for 5 min. Then right ventricular, atriums were removed, and LV sections were weighted. The pictures of LV slices were taken using a professional camera. Images were analyzed using Image-J software. Scar size percentages were calculated.

Plasma collection

The blood was drawn from the right ventricle and collected on EDTA in a microcentrifuge tube coated with EDTA. The blood was centrifuged at 4600 RPM at 4^{o}C for 10 minutes. The plasma was collected and stored at -80^{o}C till process.

Toxicity tests

The plasma level of LDH, total cholesterol, HDL-cholesterol, triglycerides, ALT, AST, Albumin, and creatinine were performed using Ace Axcel® Clinical Chemistry System (Alfa Wassermann,

West Caldwell, NJ). LDL-cholesterol was calculated using Friedewald calculation (LDL-cholesterol (mg/dL) = total cholesterol – HDL– (triglycerides/5)).

Alpha-fetoprotein (AFP) ELISA assay

The AFP levels in the plasma were detected following the manufacture protocol Rat Alpha-Fetoprotein (AFP) ELISA Kit (MyBioSource, Cat# MBS034337). In brief, the plasma samples were incubated with an antibody specific to Rat AFP-HRP conjugated for 60 minutes at 37ºC. This was followed by the addition of chromogen solution for 15 minutes at 37°C. Only those wells that contain Rat AFP will appear yellow. The reaction was then terminated using with stop solution. The optical density (OD) was measured spectrophotometrically at a wavelength of 450 nm using a Cytation 1 plate reader. The OD value is proportional to the concentration of Rat AFP. Rat AFP in the samples was calculated by comparing the OD of the samples to the standard curve.

CA-19 ELISA assay

The CA-19-9 level in the plasma was detected following the manufacture protocol Rat CA19-9 ELISA Kit (MyBioSource, Cat# MBS2515823). Briefly, the plasma was incubated on the provided microplate pre-coated with an antibody specific to Rat CA19-9 for 90 min at 37ºC. Then biotinylated detection antibodies specific for RAT CA-19-9 and Avidin-HRB conjugated were added to each well and incubated at 37ºC. Next, the substrate solution is added to each well. Only those wells that contain Rat CA19-9 will appear blue. The addition of stop solution terminates the enzyme-substrate reaction, and the color turns yellow. The optical density (OD) is measured spectrophotometrically at a wavelength of 450 nm using a Cytation 1 plate reader. The OD value is proportional to the concentration of Rat CA19-9. Rat CA19-9 in the samples was calculated by comparing the OD of the samples to the standard curve.

Apoptosis (TUNEL) assay:

TUNEL Assay was done using Click-iT™ Plus TUNEL Assay kit (Invitrogen Cat# C10619). Slides of 8µm thick heart sections were prepared as described above. To start the assay, OCT was removed by heating at 95ºC for 5 min then washing in PBS for 30 min. Slides were immersed in

4% paraformaldehyde (Electron Microscopy Sciences Cat# 15713-S) for 15 minutes at 37°C, followed by twice washing in PBS for 5 minutes each. Tissues were then incubated for 15 minutes with Proteinase K solution as a permeabilization reagent followed by a wash in PBS for 2 times 5 minutes each. The tissues were immersed in 4% paraformaldehyde for 15 minutes at 37°C followed by twice washing in PBS for 5 minutes each, then rinsed in deionized water. Afterward, TdT reaction and the visualization reaction were performed as recommended by the manufacturer protocol. The samples were blocked with 3% BSA, immunostaining protocol for troponin staining followed as described above, and nuclei stained blue with DAPI.

For positive control, DNA strand breaks were induced by incubating permeabilized cells with 1 unit of DNase I (DNase Max® kit - Qiagen Cat#15200-50) for 30minutes at 37°C.

4. Supplemental Movies

Supplementary movie 1. LacZ AurKB GFP: Time-lapse imaging of hiPS-CMs infected with AruKB-GFP reporter and LacZ adenovirus

Supplementary movie 2. 4F AurKB GFP: Time-lapse imaging of hiPS-CMs infected with AruKB-GFP reporter and 4F adenoviruses

Supplementary movie 3. LacZ Pig MRI 4 chamber view: Full cardiac cycle 4 weeks following LacZ viral injection in pig heart (4 chamber view).

Supplementary movie 4. LacZ Pig MRI short axis view: Full cardiac cycle 4 weeks following LacZ viral injection in pig heart (short axis view).

Supplementary movie 5. 4F Pig MRI 4 chamber view: Full cardiac cycle 4 weeks following 4F viral injection in pig heart (4 chamber view).

Supplementary movie 6. 4F Pig MRI short axis view: Full cardiac cycle 4 weeks following 4F viral injection in pig heart (short axis view).

5. Supplemental Source Data Excel Sheets

Source data 1. FPKM for gene expression of bulk RNAseq from hiPS-CMs and FPKM values for heat maps in fig 1 and 2

Source data 2. GO term analysis of 4F differential gene expression 48h in hiPS-CMs

Source data 3. GO term analysis of 4F differential gene expression 72h in hiPS-CMs

Source data 4. FPKM for gene expression of bulk RNAseq and FPKM values from P7 neonatal cardiomyocytes

Source data 5. GO term analysis of 4F differential gene expression in P7 neonatal cardiomyocytes

Source data 6. GO Term analysis of differentially expressed genes from single cell RNAseq Cluster 1 vs Cluster 2

Source data 7. GO Term analysis of differentially expressed genes from single cell RNAseq Cluster 1 vs Cluster 3

Source data 8. GO Term analysis of differentially expressed genes from single cell RNAseq Cluster 3 vs Cluster 5

Source data 9. GO Term analysis of differentially expressed genes from single cell RNAseq mitotic (cluster 4) vs premitotic (cluster 5)

Source data 10. GO Term analysis of differentially expressed genes from single cell RNAseq mitotic (cluster 4) vs quiescent (cluster 8)

Source data 11. GO Term analysis of differentially expressed genes from single cell RNAseq Cluster 4 vs Cluster 6

References:

23. Ma HT and Poon RY. How protein kinases co-ordinate mitosis in animal cells. *Biochem J*. 2011;435:17-31.
24. Canseco DC, Kimura W, Garg S, Mukherjee S, Bhattacharya S, Abdisalaam S, Das S, Asaithamby A, Mammen PP and Sadek HA. Human ventricular unloading induces cardiomyocyte proliferation. *J Am Coll Cardiol*. 2015;65:892-900.
25. Hesse M, Doengi M, Becker A, Kimura K, Voeltz N, Stein V and Fleischmann BK. Midbody Positioning and Distance Between Daughter Nuclei Enable Unequivocal Identification of Cardiomyocyte Cell Division in Mice. *Circ Res*. 2018;123:1039-1052.
26. Jiang J, Burgon PG, Wakimoto H, Onoue K, Gorham JM, O'Meara CC, Fomovsky G, McConnell BK, Lee RT, Seidman JG, et al. Cardiac myosin binding protein C regulates postnatal myocyte cytokinesis. *Proc Natl Acad Sci U S A*. 2015;112:9046-51.
27. Kimura M, Uchida C, Takano Y, Kitagawa M and Okano Y. Cell cycle-dependent regulation of the human aurora B promoter. *Biochem Biophys Res Commun*. 2004;316:930-6.
28. Sadek H and Olson EN. Toward the Goal of Human Heart Regeneration. *Cell Stem Cell*. 2020;26:7-16.
29. Cauquil M, Mias C, Guilbeau-Frugier C, Karsenty C, Seguelas M-H, Genet G, Renaud-Gabardos E, Prats A-C, Pons V, Branchereau M, et al. Ephrin-B1 blocks adult cardiomyocyte proliferation and heart regeneration. *bioRxiv*. *Preprint posted online August 15, 2019. https://doi.org/10.1101/735571.*
30. Monroe TO, Hill MC, Morikawa Y, Leach JP, Heallen T, Cao S, Krijger PHL, de Laat W, Wehrens XHT, Rodney GG, et al. YAP Partially Reprograms Chromatin Accessibility to Directly Induce Adult Cardiogenesis In Vivo. *Dev Cell*. 2019;48:765-779 e7.
31. Nguyen NUN, Canseco DC, Xiao F, Nakada Y, Li S, Lam NT, Muralidhar SA, Savla JJ, Hill JA, Le V, et al. A calcineurin-Hoxb13 axis regulates growth mode of mammalian cardiomyocytes. *Nature*. 2020;582:271-276.
32. Pettinato AM, Yoo D, VanOudenhove J, Chen YS, Cohn R, Ladha FA, Yang X, Thakar K, Romano R, Legere N, et al. Sarcomere function activates a p53-dependent DNA damage response that promotes polyploidization and limits in vivo cell engraftment. *Cell Rep*. 2021;35:109088.
33. Abouleisa RRE, McNally L, Salama ABM, Hammad SK, Ou Q, Wells C, Lorkiewicz PK, Bolli R, Mohamed TMA and Hill BG. Cell cycle induction in human cardiomyocytes is dependent on biosynthetic pathway activation. *Redox Biol*. 2021;46:102094.
34. Magadum A, Singh N, Kurian AA, Munir I, Mehmood T, Brown K, Sharkar MTK, Chepurko E, Sassi Y, Oh JG, et al. Pkm2 regulates cardiomyocyte cell cycle and promotes cardiac regeneration. *Circulation*. 2020; 141(15):1249-1265.
35. Honkoop H, de Bakker DE, Aharonov A, Kruse F, Shakked A, Nguyen PD, de Heus C, Garric L, Muraro MJ, Shoffner A, et al. Single-cell analysis uncovers that metabolic reprogramming by ErbB2 signaling is essential for cardiomyocyte proliferation in the regenerating heart. *Elife*. 2019; 8:e50163.
36. Cardoso AC, Lam NT, Savla JJ, Nakada Y, Pereira AHM, Elnwasany A, Menendez-Montes I, Ensley EL, Petric UB, Sharma G, et al. Mitochondrial substrate utilization regulates cardiomyocyte cell-cycle progression. *Nature Metabolism*. 2020;2:167-178.
37. Bae J, Salamon RJ, Brandt EB, Paltzer WG, Zhang Z, Britt EC, Hacker TA, Fan J and Mahmoud AI. Malonate Promotes Adult Cardiomyocyte Proliferation and Heart Regeneration. *Circulation*. 2021; 143(20):1973-1986.
38. Mills RJ, Parker BL, Quaife-Ryan GA, Voges HK, Needham EJ, Bornot A, Ding M, Andersson H, Polla M, Elliott DA, et al. Drug Screening in Human PSC-Cardiac Organoids Identifies Pro-proliferative Compounds Acting via the Mevalonate Pathway. *Cell Stem Cell*. 2019;24:895-907 e6.

39. Tran DH and Wang ZV. Glucose Metabolism in Cardiac Hypertrophy and Heart Failure. *J Am Heart Assoc*. 2019;8:e012673.
40. Gabisonia K, Prosdocimo G, Aquaro GD, Carlucci L, Zentilin L, Secco I, Ali H, Braga L, Gorgodze N, Bernini F, et al. MicroRNA therapy stimulates uncontrolled cardiac repair after myocardial infarction in pigs. *Nature*. 2019;569:418-422.
41. Mohamed TMA, Ang YS, Radzinsky E, Zhou P, Huang Y, Elfenbein A, Foley A, Magnitsky S and Srivastava D. Regulation of Cell Cycle to Stimulate Adult Cardiomyocyte Proliferation and Cardiac Regeneration. *Cell*. 2018;173:104-116 e12.
42. Ou Q, Jacobson Z, Abouleisa RRE, Tang XL, Hindi SM, Kumar A, Ivey KN, Giridharan G, El-Baz A, Brittian K, et al. Physiological Biomimetic Culture System for Pig and Human Heart Slices. *Circ Res*. 2019;125:628-642.
43. Bassat E, Mutlak YE, Genzelinakh A, Shadrin IY, Baruch Umansky K, Yifa O, Kain D, Rajchman D, Leach J, Riabov Bassat D, et al. The extracellular matrix protein agrin promotes heart regeneration in mice. *Nature*. 2017;547:179-184.
44. Heallen T, Zhang M, Wang J, Bonilla-Claudio M, Klysik E, Johnson RL and Martin JF. Hippo pathway inhibits Wnt signaling to restrain cardiomyocyte proliferation and heart size. *Science*. 2011;332:458-61.
45. Morikawa Y, Zhang M, Heallen T, Leach J, Tao G, Xiao Y, Bai Y, Li W, Willerson JT and Martin JF. Actin cytoskeletal remodeling with protrusion formation is essential for heart regeneration in Hippo-deficient mice. *Sci Signal*. 2015;8:ra41.
46. Chaudhry HW, Dashoush NH, Tang H, Zhang L, Wang X, Wu EX and Wolgemuth DJ. Cyclin A2 mediates cardiomyocyte mitosis in the postmitotic myocardium. *J Biol Chem*. 2004;279:35858-66.
47. Cheng RK, Asai T, Tang H, Dashoush NH, Kara RJ, Costa KD, Naka Y, Wu EX, Wolgemuth DJ and Chaudhry HW. Cyclin A2 induces cardiac regeneration after myocardial infarction and prevents heart failure. *Circ Res*. 2007;100:1741-8.
48. Shapiro SD, Ranjan AK, Kawase Y, Cheng RK, Kara RJ, Bhattacharya R, Guzman-Martinez G, Sanz J, Garcia MJ and Chaudhry HW. Cyclin A2 induces cardiac regeneration after myocardial infarction through cytokinesis of adult cardiomyocytes. *Sci Transl Med*. 2014;6:224ra27.
49. Woo YJ, Panlilio CM, Cheng RK, Liao GP, Atluri P, Hsu VM, Cohen JE and Chaudhry HW. Therapeutic delivery of cyclin A2 induces myocardial regeneration and enhances cardiac function in ischemic heart failure. *Circulation*. 2006;114:I206-13.
50. Lane AN and Fan TWM. Regulation of mammalian nucleotide metabolism and biosynthesis. *Nucleic Acids Research*. 2015;43:2466-2485.
51. Cui M, Wang Z, Chen K, Shah AM, Tan W, Duan L, Sanchez-Ortiz E, Li H, Xu L, Liu N, et al. Dynamic Transcriptional Responses to Injury of Regenerative and Non-regenerative Cardiomyocytes Revealed by Single-Nucleus RNA Sequencing. *Dev Cell*. 2020;53:102-116 e8.
52. Cui M, Atmanli A, Morales MG, Tan W, Chen K, Xiao X, Xu L, Liu N, Bassel-Duby R and Olson EN. Nrf1 promotes heart regeneration and repair by regulating proteostasis and redox balance. *Nat Commun*. 2021;12:5270.
53. Zangi L, Lui KO, von Gise A, Ma Q, Ebina W, Ptaszek LM, Später D, Xu H, Tabebordbar M, Gorbatov R, et al. Modified mRNA directs the fate of heart progenitor cells and induces vascular regeneration after myocardial infarction. *Nat Biotechnol*. 2013;31:898-907.
54. Shaw A and Cornetta K. Design and Potential of Non-Integrating Lentiviral Vectors. *Biomedicines*. 2014;2:14-35.
55. Milone MC and O'Doherty U. Clinical use of lentiviral vectors. *Leukemia*. 2018; 32(7):1529-1541.
56. Zhao M, Nakada Y, Wei Y, Bian W, Chu Y, Borovjagin AV, Xie M, Zhu W, Nguyen T, Zhou Y, et al. Cyclin D2 Overexpression Enhances the Efficacy of Human Induced Pluripotent

Stem Cell-Derived Cardiomyocytes for Myocardial Repair in a Swine Model of Myocardial Infarction. *Circulation*. 2021;144:210-228.
57. Mohamed TM, Stone NR, Berry EC, Radzinsky E, Huang Y, Pratt K, Ang YS, Yu P, Wang H, Tang S, et al. Chemical Enhancement of In Vitro and In Vivo Direct Cardiac Reprogramming. *Circulation*. 2017;135:978-995.
58. Bradley LA, Young A, Li H, Billcheck HO and Wolf MJ. Loss of Endogenously Cycling Adult Cardiomyocytes Worsens Myocardial Function. *Circ Res*. 2021;128:155-168.
59. Sultana N, Magadum A, Hadas Y, Kondrat J, Singh N, Youssef E, Calderon D, Chepurko E, Dubois N, Hajjar RJ, et al. Optimizing Cardiac Delivery of Modified mRNA. *Mol Ther*. 2017;25:1306-1315.
60. Mohamed TM, Oceandy D, Prehar S, Alatwi N, Hegab Z, Baudoin FM, Pickard A, Zaki AO, Nadif R, Cartwright EJ, et al. Specific role of neuronal nitric-oxide synthase when tethered to the plasma membrane calcium pump in regulating the beta-adrenergic signal in the myocardium. *J Biol Chem*. 2009;284:12091-8.
61. Stuart T, Butler A, Hoffman P, Hafemeister C, Papalexi E, Mauck WM, 3rd, Hao Y, Stoeckius M, Smibert P and Satija R. Comprehensive Integration of Single-Cell Data. *Cell*. 2019;177:1888-1902 e21.
62. Cao J, Spielmann M, Qiu X, Huang X, Ibrahim DM, Hill AJ, Zhang F, Mundlos S, Christiansen L, Steemers FJ, et al. The single-cell transcriptional landscape of mammalian organogenesis. *Nature*. 2019;566:496-502.
63. Kiselev VY, Yiu A and Hemberg M. scmap: projection of single-cell RNA-seq data across data sets. *Nat Methods*. 2018;15:359-362.
64. Mehra P, Guo Y, Nong Y, Lorkiewicz P, Nasr M, Li Q, Muthusamy S, Bradley JA, Bhatnagar A, Wysoczynski M, et al. Cardiac mesenchymal cells from diabetic mice are ineffective for cell therapy-mediated myocardial repair. *Basic Res Cardiol*. 2018;113:46.
65. Li Q, Guo Y, Ou Q, Wu WJ, Chen N, Zhu X, Tan W, Yuan F, Dawn B, Luo L, et al. Gene transfer as a strategy to achieve permanent cardioprotection II: rAAV-mediated gene therapy with heme oxygenase-1 limits infarct size 1 year later without adverse functional consequences. *Basic Res Cardiol*. 2011;106:1367-77.
66. Tang XL, Nakamura S, Li Q, Wysoczynski M, Gumpert AM, Wu WJ, Hunt G, Stowers H, Ou Q and Bolli R. Repeated Administrations of Cardiac Progenitor Cells Are Superior to a Single Administration of an Equivalent Cumulative Dose. *J Am Heart Assoc*. 2018; 7(4):e007400.
67. Tokita Y, Tang XL, Li Q, Wysoczynski M, Hong KU, Nakamura S, Wu WJ, Xie W, Li D, Hunt G, et al. Repeated Administrations of Cardiac Progenitor Cells Are Markedly More Effective Than a Single Administration: A New Paradigm in Cell Therapy. *Circ Res*. 2016;119:635-51.
68. Bolli R, Tang XL, Sanganalmath SK, Rimoldi O, Mosna F, Abdel-Latif A, Jneid H, Rota M, Leri A and Kajstura J. Intracoronary delivery of autologous cardiac stem cells improves cardiac function in a porcine model of chronic ischemic cardiomyopathy. *Circulation*. 2013;128:122-31.
69. Swindle MM, Smith AC and Hepburn BJ. Swine as models in experimental surgery. *J Invest Surg*. 1988;1:65-79.
70. Swindle MM, Horneffer PJ, Gardner TJ, Gott VL, Hall TS, Stuart RS, Baumgartner WA, Borkon AM, Galloway E and Reitz BA. Anatomic and anesthetic considerations in experimental cardiopulmonary surgery in swine. *Lab Anim Sci*. 1986;36:357-61.

Supplemental Fig. 1

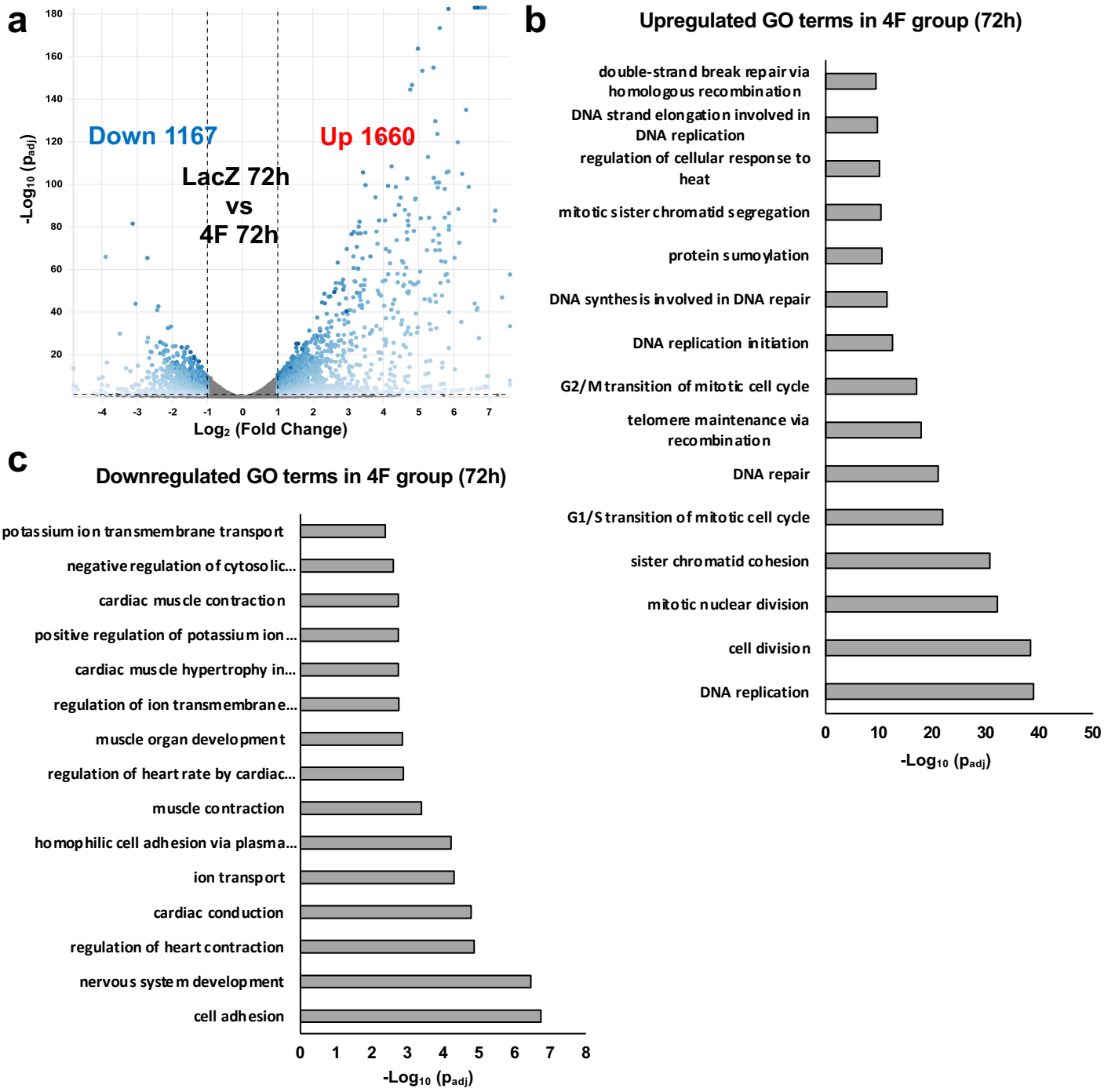

Supplemental Fig. 1: Differential gene expression 72h post 4F overexpression maintains most of the 48 h phenotype of induced cell cycle reprogramming. (a) Volcano plot demonstrating the number of genes that are significantly upregulated or downregulated 72 h post-4F adenovirus overexpression compared to the LacZ group (p_{adj}<0.05). **(b)** The bar graph shows the top 15 GO terms for the significantly upregulated genes from RNA-seq data comparing hiPS-CMs infected with either LacZ or 4F for 72 h (p_{adj}<0.05). The GO terms reflect mostly upregulation of cell cycle genes. **(c)** The bar graph shows the top 15 GO terms for the significantly downregulated genes from RNA-seq data comparing gene expression between the hiPS-CMs infected with either LacZ or 4F for 72 h (p_{adj}<0.05). The GO terms reflect the downregulation of cardiac contractile and sarcomeric genes. Source data 1 lists FPKM values for all RNAseq data and for the heart maps. Source data 3 contains the full list of the GO terms and the genes included in each GO term.

Supplemental Fig. 2

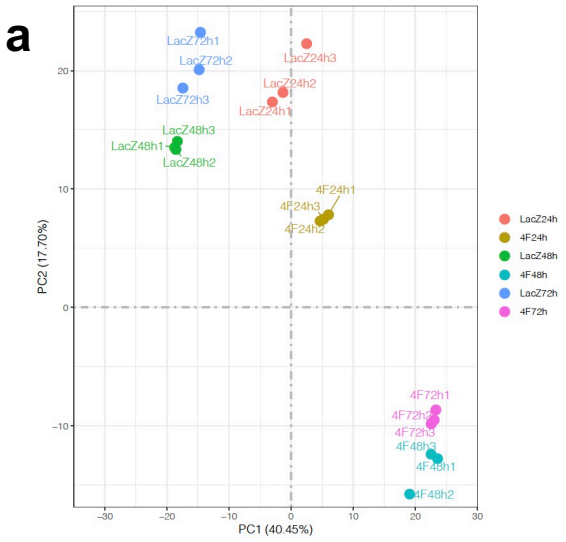

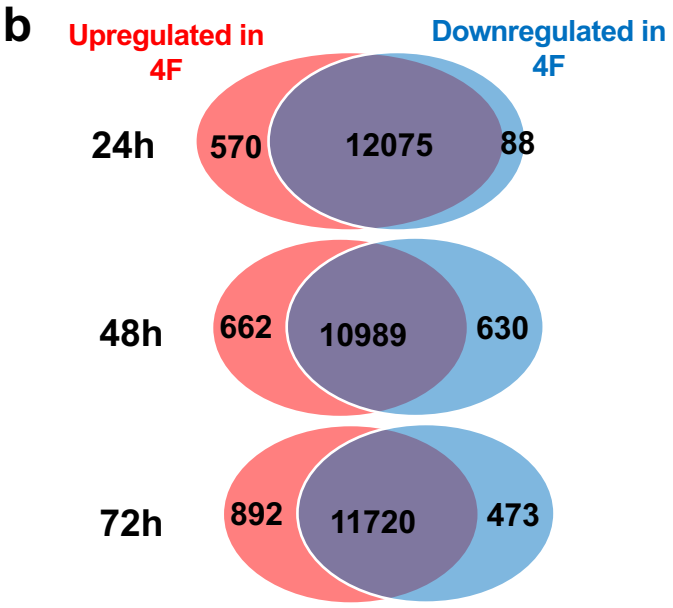

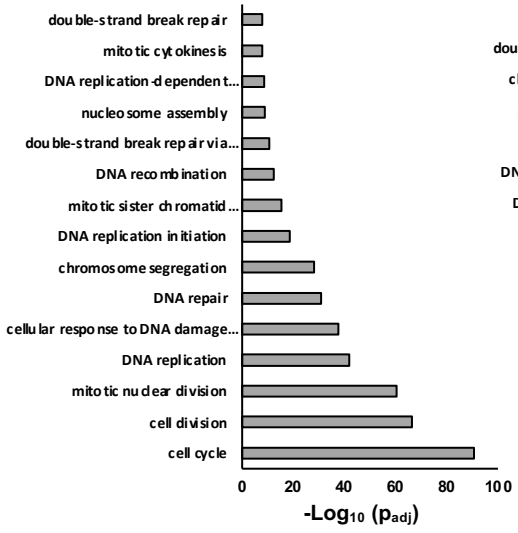

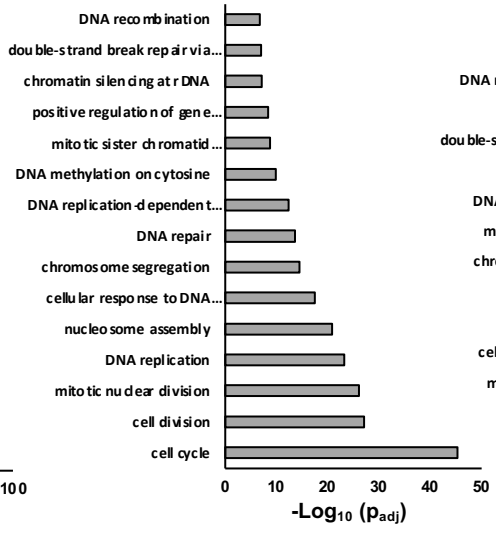

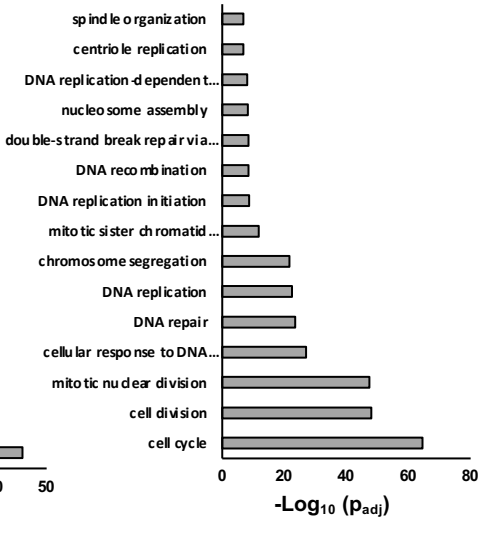

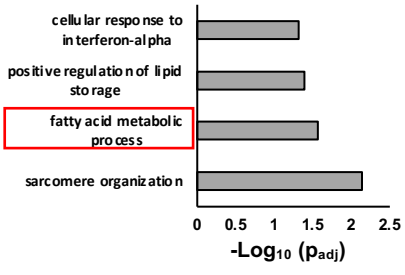

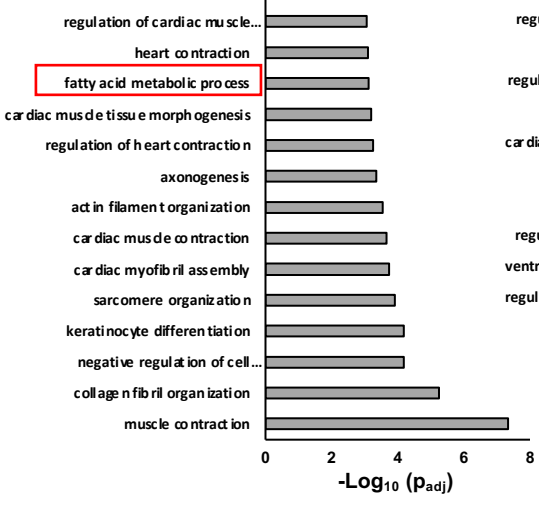

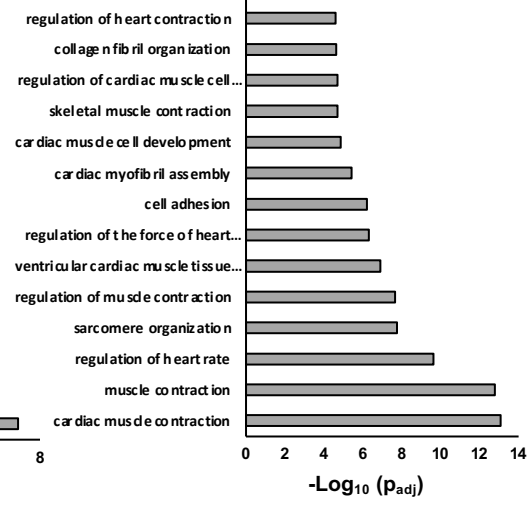

Supplemental Fig. 2. 4F overexpression induces cell cycle reprogramming in P7 neonatal cardiomyocytes. **(a)** Principal component analysis (PCA) of RNA-seq data from P7 neonatal cardiomyocytes infected with either LacZ (control) or 4F for 24, 48, or 72 h (n = 3). **(b)** Venn diagrams demonstrating the number of genes that are significantly upregulated or downregulated at each time point post-4F adenovirus overexpression compared to the LacZ group (p_{adj}<0.05). Bar graphs show the top GO terms for the significantly upregulated or downregulated genes from RNA-seq data comparing P7 neonatal cardiomyocytes infected with either LacZ or 4F for 24 h **(c-d)**, 48h **(e-f),** or 72h **(g-h)** (p_{adj}<0.05). The GO terms reflect mostly upregulation of cell cycle genes and downregulation of the sarcomeric genes at 48 and 72 h time points similar to the hiPS-CMs (n=3 in each sample). Source data 4 lists FPKM values for all RNAseq data and for the heart maps. Source data 5 contains the full list of the GO terms and the genes included in each GO term.

Supplemental Fig. 3

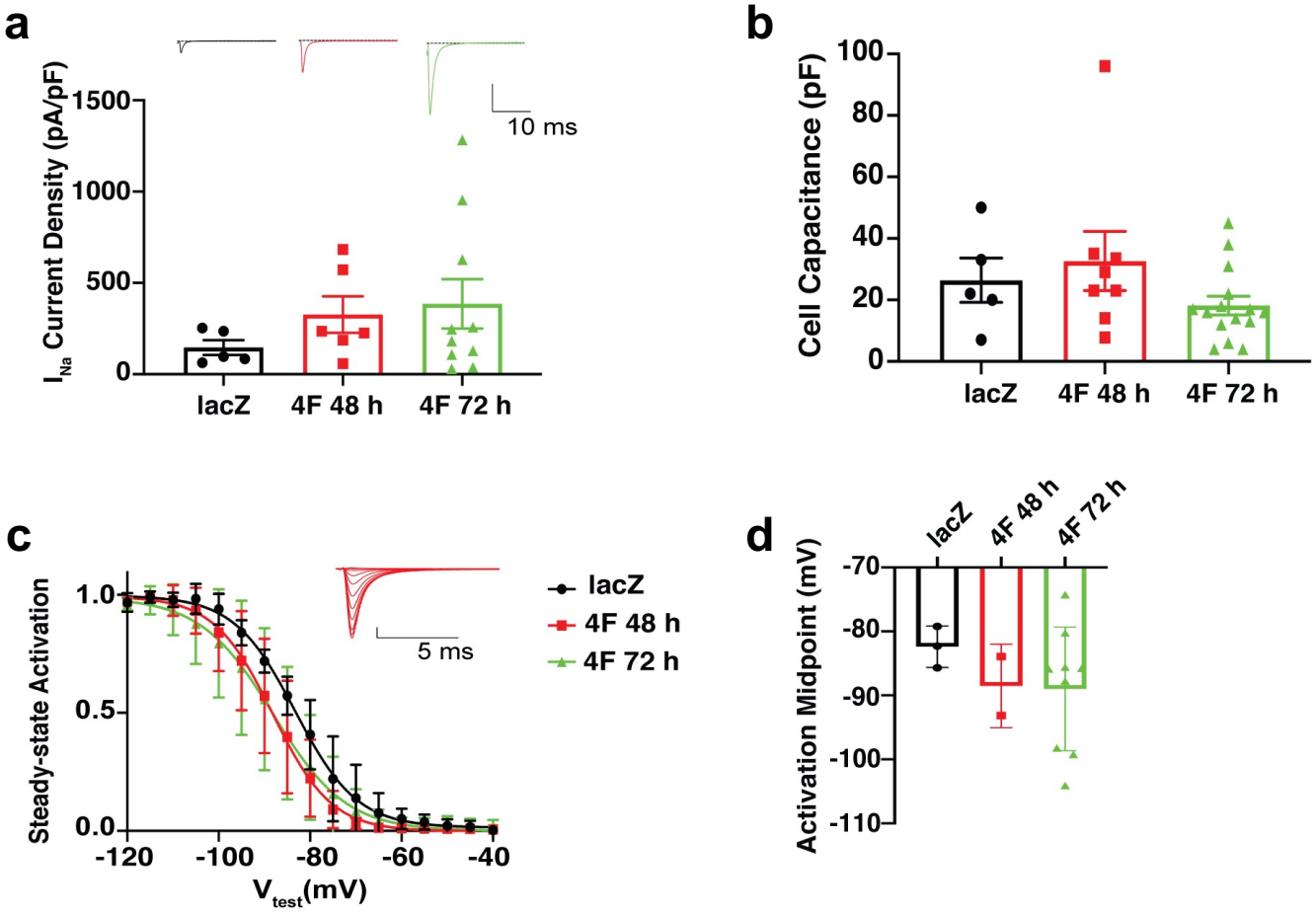

Supplemental Fig. 3. 4F infection of hiPS-CMs does not significantly change I_{Na}.
(a) Peak I_{Na} current density in lacZ (black), 48 h (red), and 72 h (green) after virus infection with 4F, with exemplar Na^+ current recorded from a V_{hold} 120mV to V_{test} 0mV. Scale bar=0.5 nA/pF, 10 ms. **(b)** Cell capacitance was not different between lacZ, and 4F treated cells either at 48 h or 72 h after infection (Compared to lacZ: 48 h p = 0.74; 72 h p=0.56). **(c)** Inset, a representative family of traces taken at 48 h after infection with 4F. Scale bar: 2 nA, 5 ms. Quantification of the steady-state activation curve demonstrates a trend towards a negative shift of steady-state inactivation midpoint, quantified in **(d).** lacZ: n = 5 cells; 4F 48 h: n = 6 cells; 4F 72 h: n =15 cells.

Supplemental Fig. 4

a

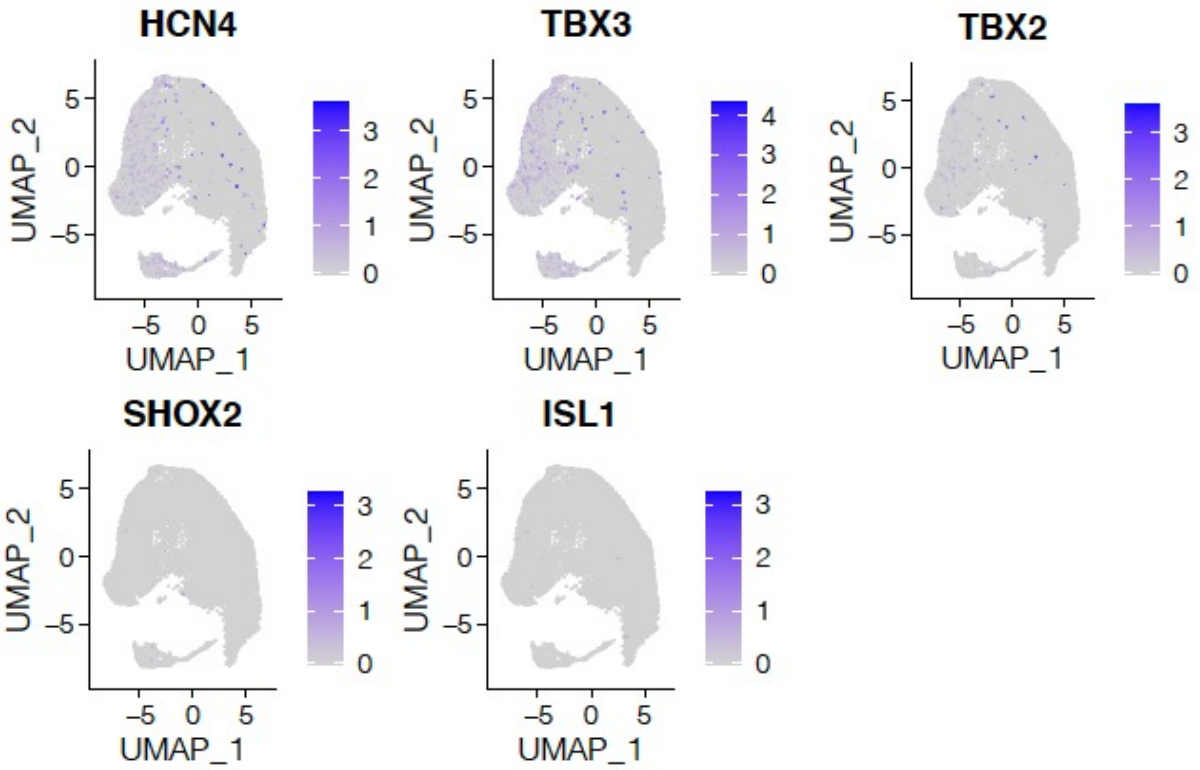

b

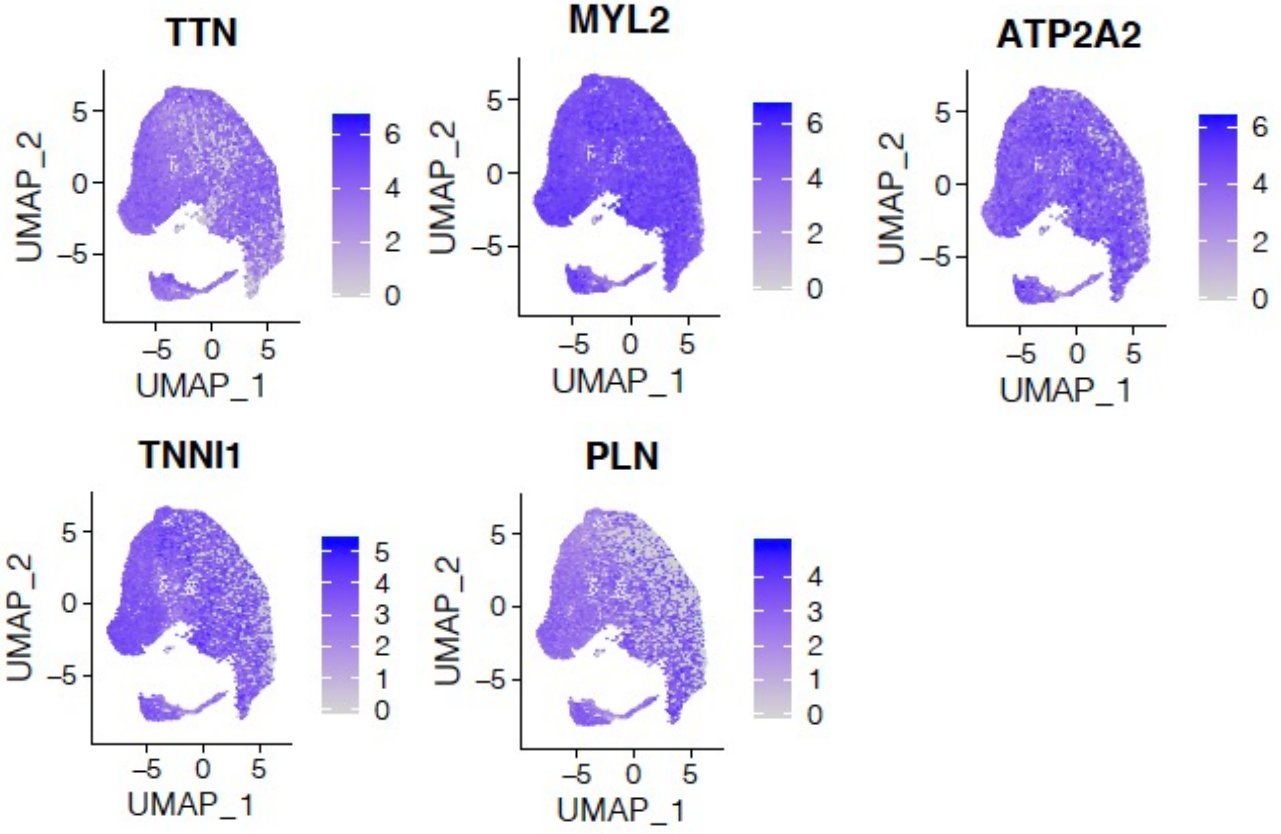

Supplemental Fig. 4. Expression of atrial, nodal and ventricular genes in hiPS-CMs used for single cell RNAseq

UMAP plots showing the expression of **(a)** atrial/nodal genes (HCN4, TBX3, TBX2, SHOX2 and ISL1) or **(b)** ventricular genes (TTN, MYL2, ATP2A2, TNNI1, and PLN) for the cells used in single cell RNAseq. The cardiomyocytes showed minimal expression of these atrial/nodal genes and major expression of the ventricular genes.

Supplemental Fig. 5

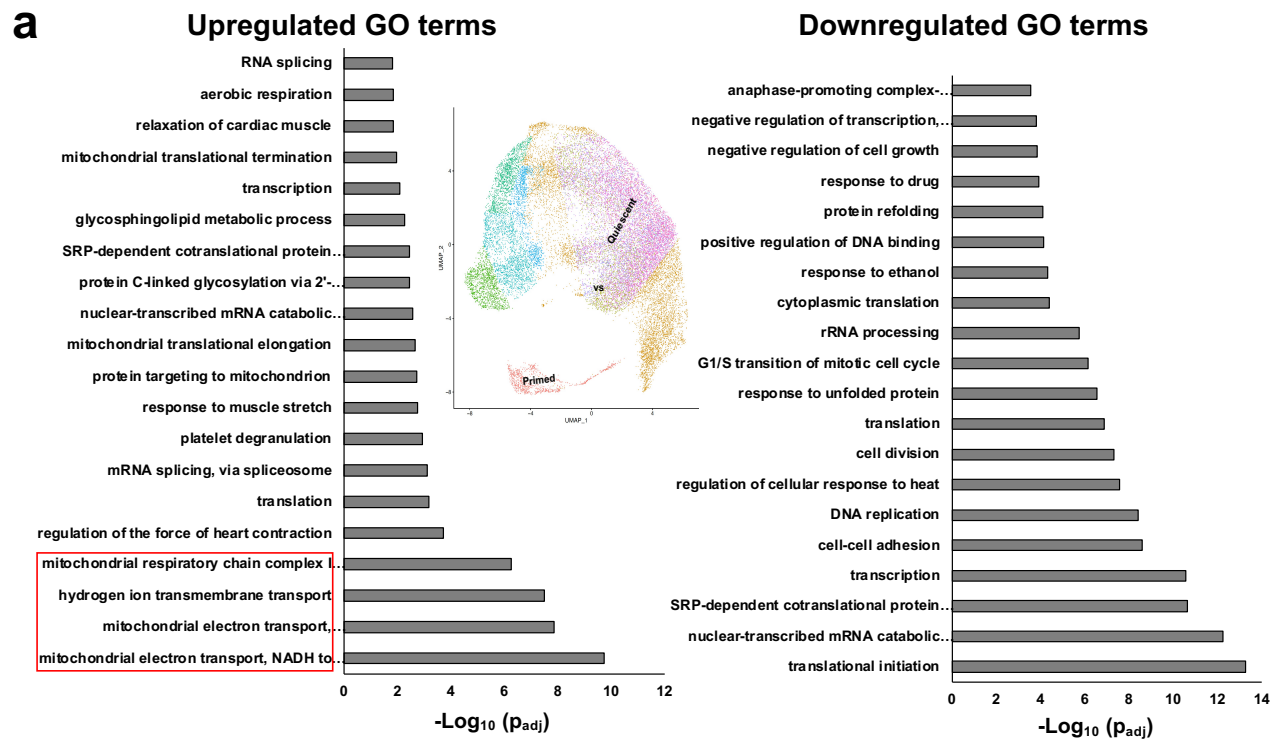

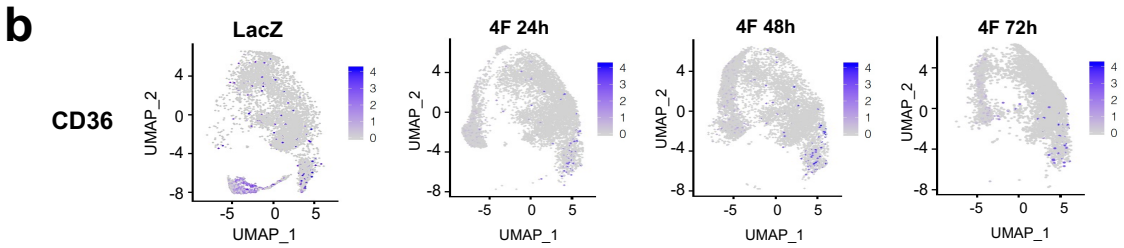

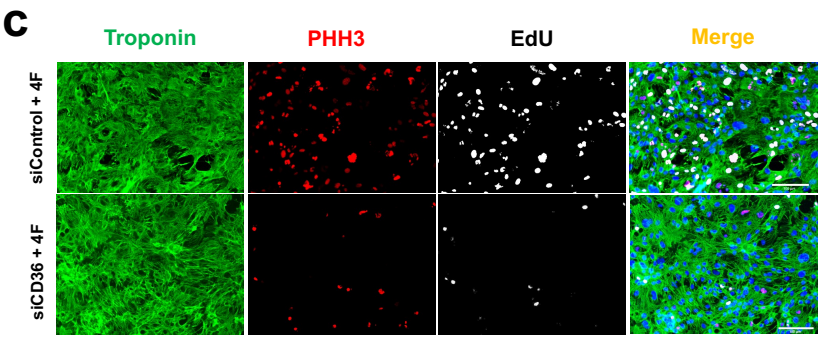

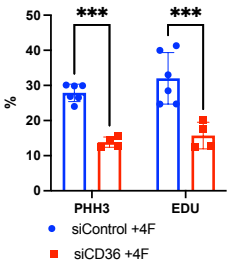

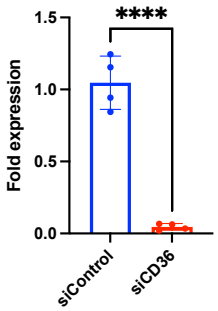

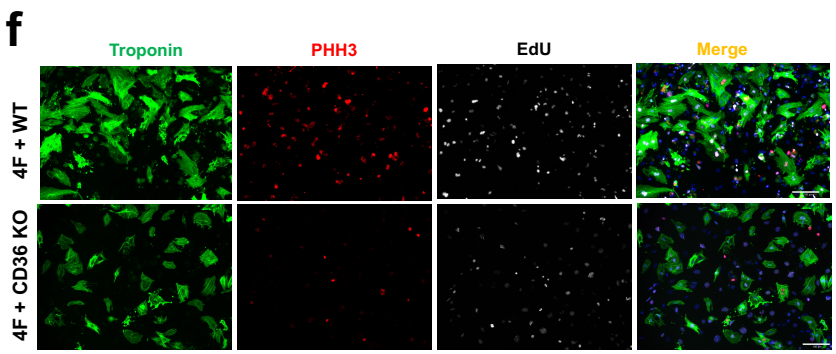

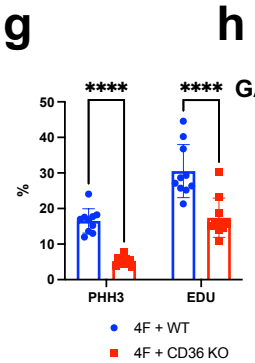

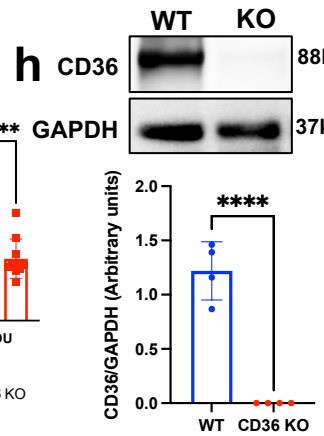

Supplemental Fig. 5. Single cell RNA-Seq data suggesting a population of myocytes that are metabolically primed for proliferation. (a) bar graphs show the up-regulated (left panel) and downregulated (right panel) GO terms in cluster 1 (primed) compared with cluster 2 (quiescent) cell population. The upregulated GO terms are focused on mitochondrial energy production. Source data 6 lists the differentially expressed genes and the full list of the GO terms and the genes included in each GO term. **(b)** UMAP plots showing the cluster 1 uniquely expressing CD36. **(c)** Representative images of hiPS-CMs infected with either siRNA targeting CD36 or scrambles control for 36 hours and followed by 4F adenoviruses for 48 h, and immuno-stained for troponin-T (green), PHH3 (red), EDU (gray) (scale bar=100μm). **(d)** Quantification of percentage of cardiomyocytes stained positive for the cell cycle markers (PHH3 and EDU) (n=4-6, ***P<0.001 vs. siControl, error bars indicate the S.D.). **(e)** Quantification of CD36 RNA expression following siRNA knockdown (n=4 ****P<0.0001 vs. siControl, error bars indicate the S.D.). **(f)** Representative images of P7 primary cardiomyocytes isolated from WT or CD36 knockout mice and infected with 4F adenoviruses for 48 h, and immuno-stained for troponin-T (green), PHH3 (red), EDU (gray) (scale bar=100μm). **(g)** Quantification of percentage of cardiomyocytes that are positive for cell cycle markers (PHH3 and EDU) (n=10, ****P<0.0001 vs. WT, error bars indicate the S.D.). **(h)** Western blot and quantification of CD36 expression in P7 mouse hearts from WT and CD36 knockouts (n=6 ****P<0.0001 vs. WT, error bars indicate the S.D.).

Supplemental Fig. 6

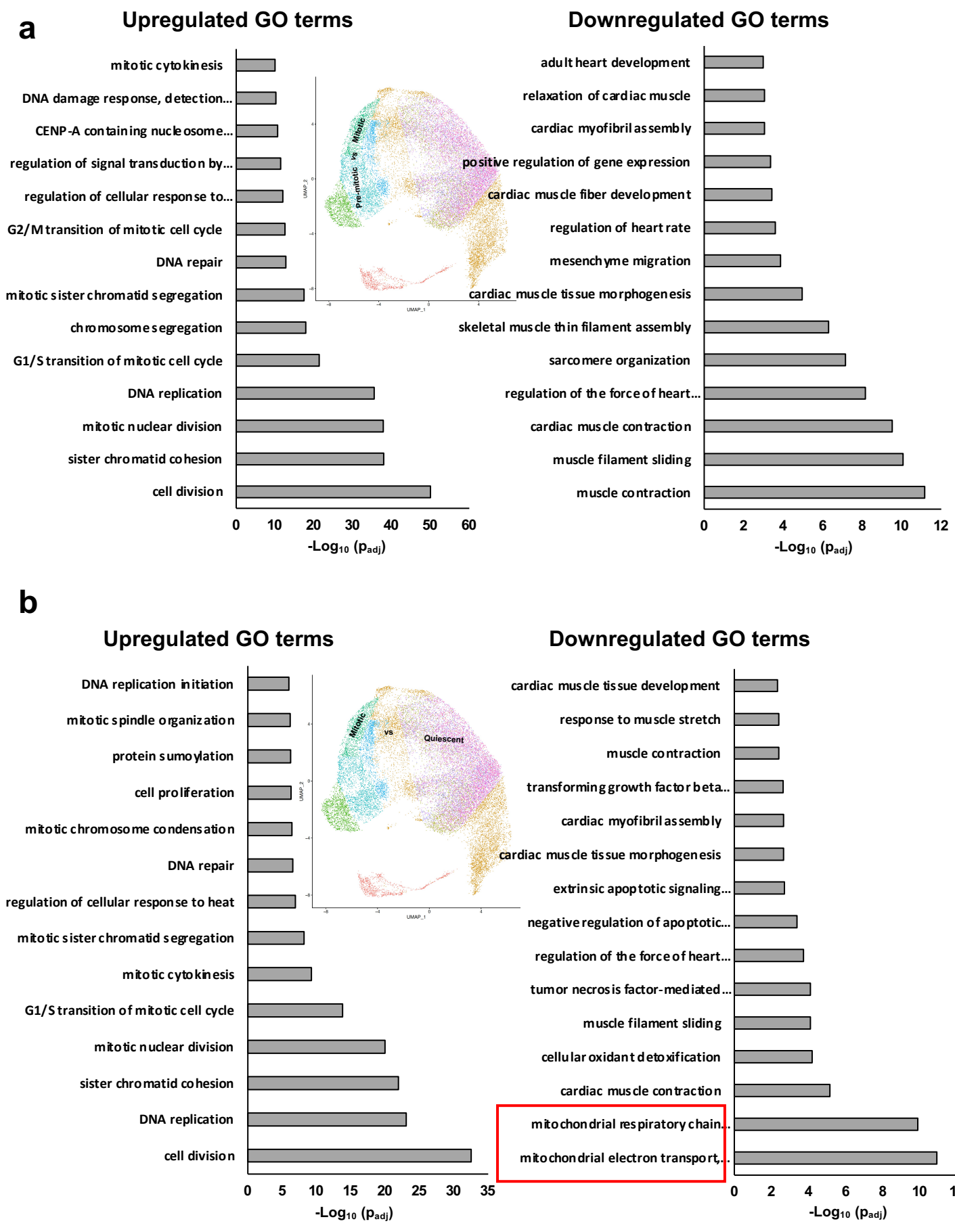

Supplemental Fig. 6. GO terms for differentially expressed genes between mitotic cardiomyocytes and pre-mitotic or quiescent cardiomyocytes 48 h post-infection with 4F.

GO terms for up- and down-regulated genes in the mitotic subpopulation compared with **(a)** the pre-mitotic subpopulation or **(b)** the quiescent subpopulation from the same sample (highlighted in the UMAP plot). Interestingly, the top downregulated GO terms in the mitotic subpopulation compared to the quiescent subpopulation involve mitochondrial electron transport chain genes in addition to the sarcomeric and cardiac contractile genes. Source data 9 and 10 list the differentially expressed genes and the full list of the GO terms and the genes included in each GO term.

Supplemental Fig. 7

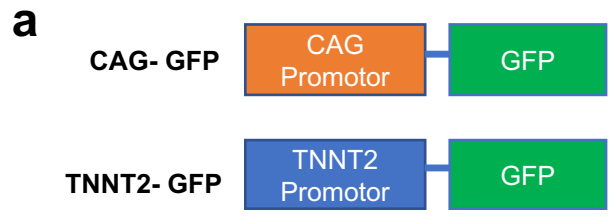

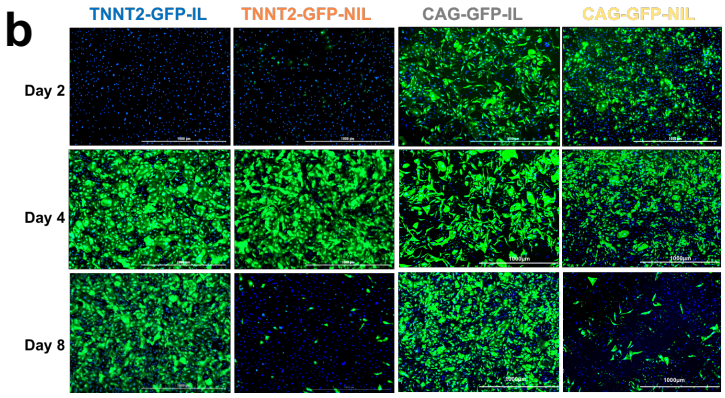

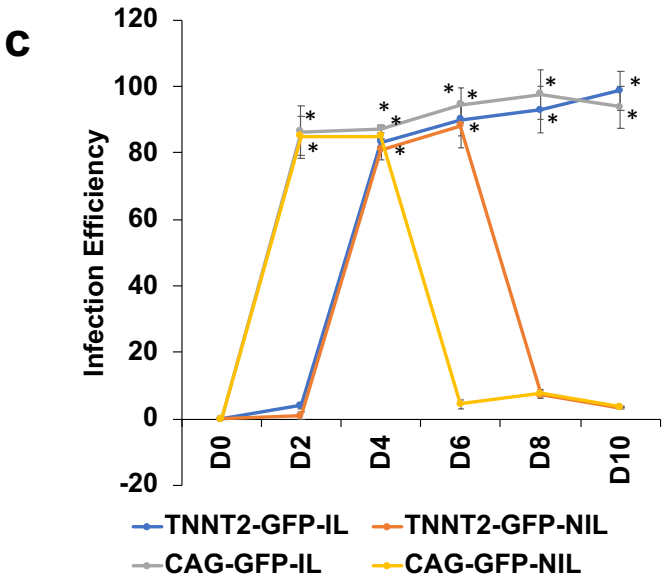

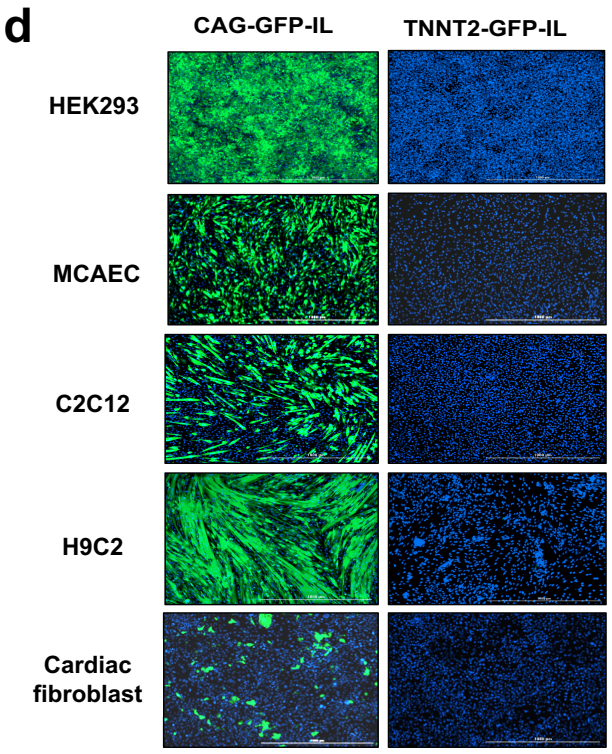

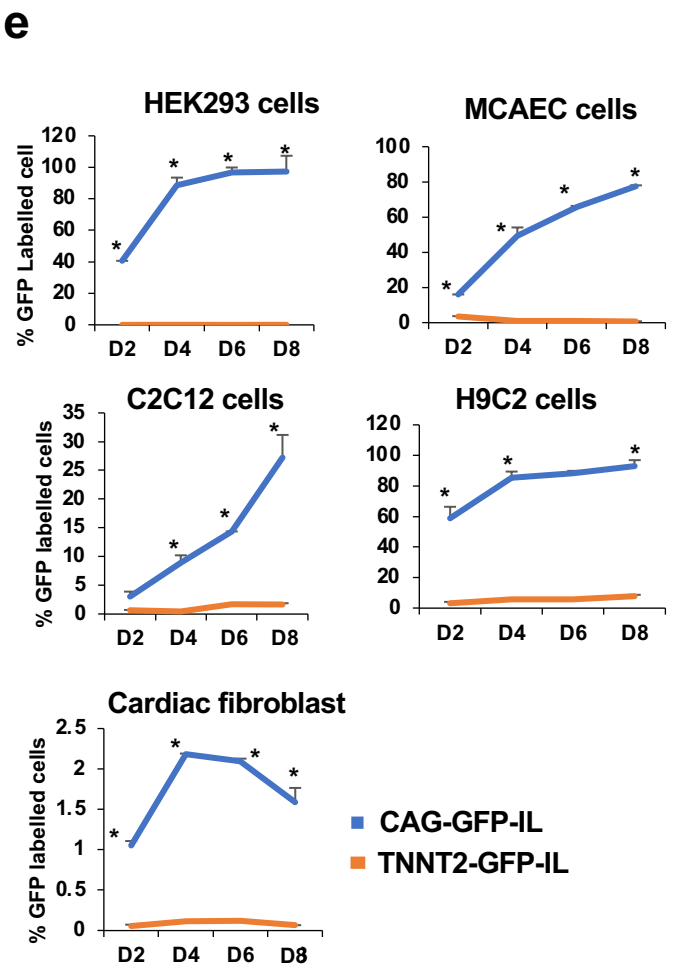

Supplemental Fig. 7. TNNT2 promoter does not drive the protein expression in other cell types.
(a) Schematic diagram of the plasmid design. **(b)** Representative live-cell images of hiPS-CMs treated with TNNT2-GFP-IL, TNNT2-GFP-NIL, CAG-GFP-IL, or CAG-GFP-NIL for 2, 4, 8 days (Scale bar=1000μm). **(c)** Quantification of GFP expression per 100 nuclei (or infection efficiency) (n=3 independent experiments conducted in duplicate, *P<0.05 vs. day 0 expression). **(d)** Representative live-cell images to show GFP expression (green) and nuclei (blue) in kidney cells (HEK293), mouse coronary artery endothelial cells (MCAEC), muscle cells (H9C2 and C2C12 myoblasts), and cardiac fibroblasts infected with CAG-GFP-IL (left panel) or TNNT2-GFP-IL (right panel) for four days (Scale bar= 1000μm). **(e)** Quantification of GFP expression per 100 nuclei for 2, 4, 6, or 8 days post-infection. (n=2 independent experiments conducted in duplicate, *p<0.05 compared to TNNT2-GFP-IL).

Supplemental Fig. 8

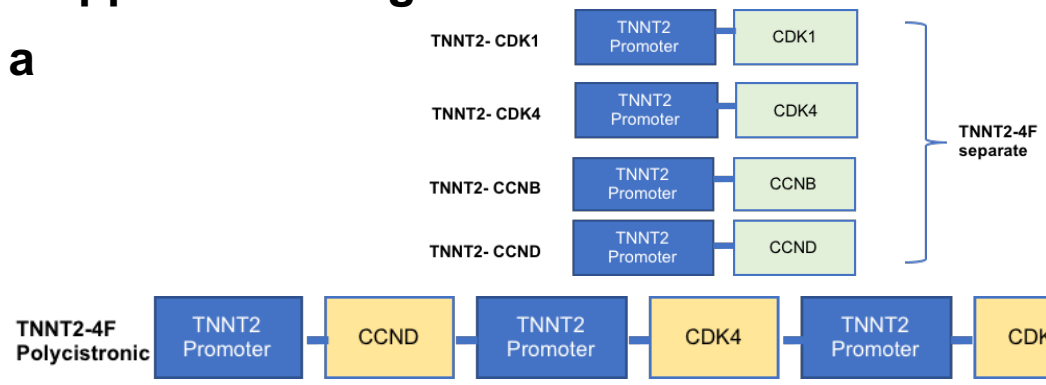

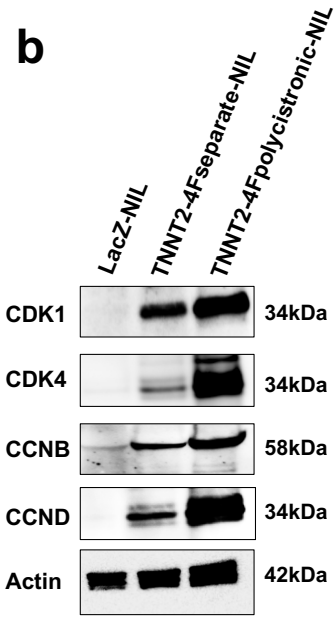

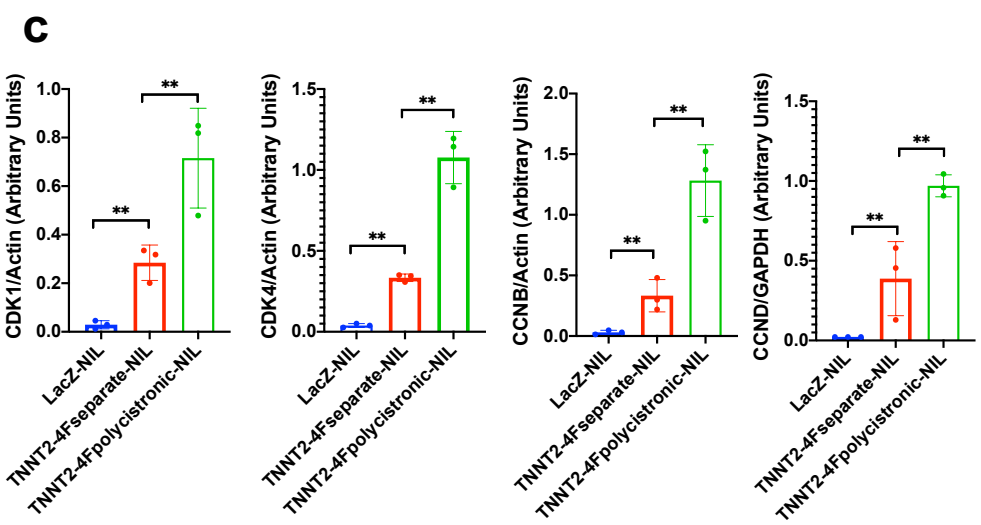

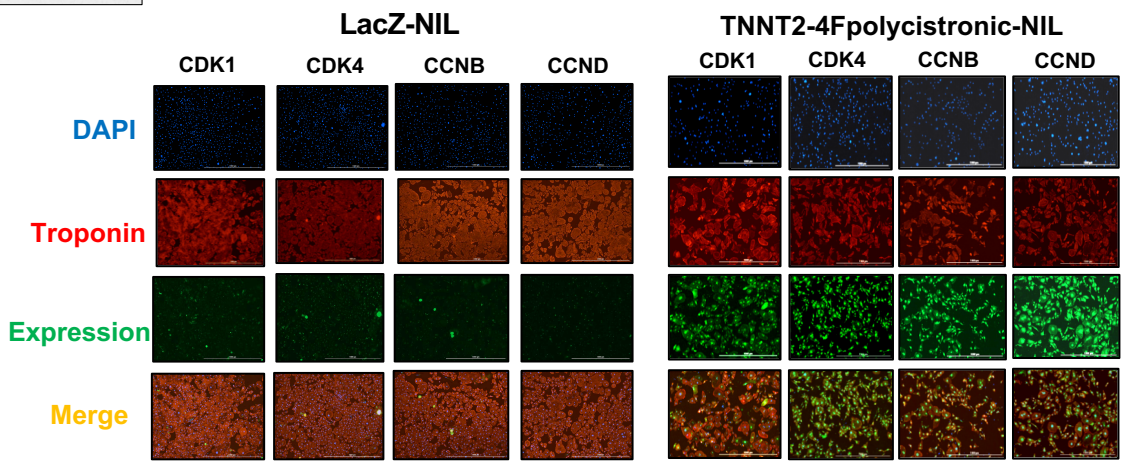

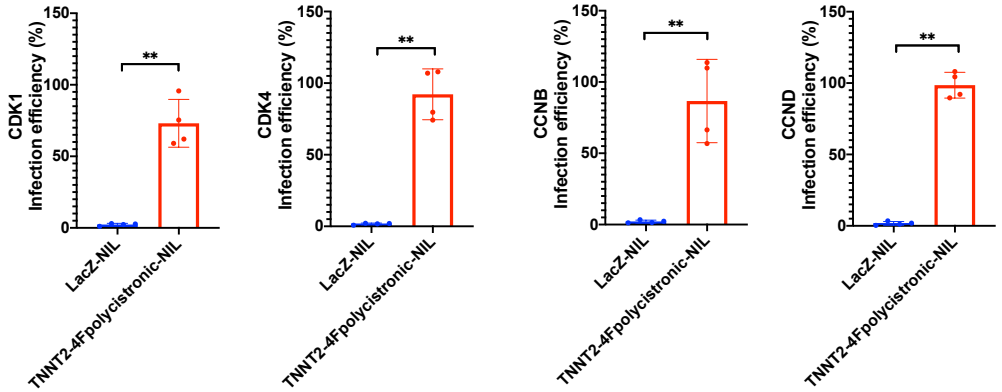

Supplemental Fig. 8. TNNT2-4Fpolycistronic-NIL efficiently drives 4F protein expression in hiPS-CMs

(a) Schematic diagram of the plasmid design for TNNT2-4Fseparate (Top panel) and TNNT2-4F polycistronic (Bottom panel). **(b)** Representative Western blots from protein lysates of hiPS-CMs treated with LacZ-NIL, TNNT2-4Fseparate-NIL, or TNNT2-4Fpolycistronic-NIL for four days to demonstrate the protein expression of the cell cycle factors. **(c)** Quantification of the protein expression of each cell cycle factor (n=3 independent experiment, **p<0.01 compared to the LacZ-NIL control group, error bars indicate the S.D.). **(d)** Representative images of hiPS-CMs treated with LacZ-NIL, or TNNT2-4Fpolycistronic-NIL for four days and stained with antibody against troponin-T (red), or the specified cell cycle factor protein expression (green) (Scale bar=1000μm). **(e)** Quantification of the infection efficiency of each cell cycle factor (n=2 independent experiment conducted in duplicate, **p<0.01 compared to the LacZ-NIL control group, error bars indicate the S.D.).

Supplemental Fig. 9

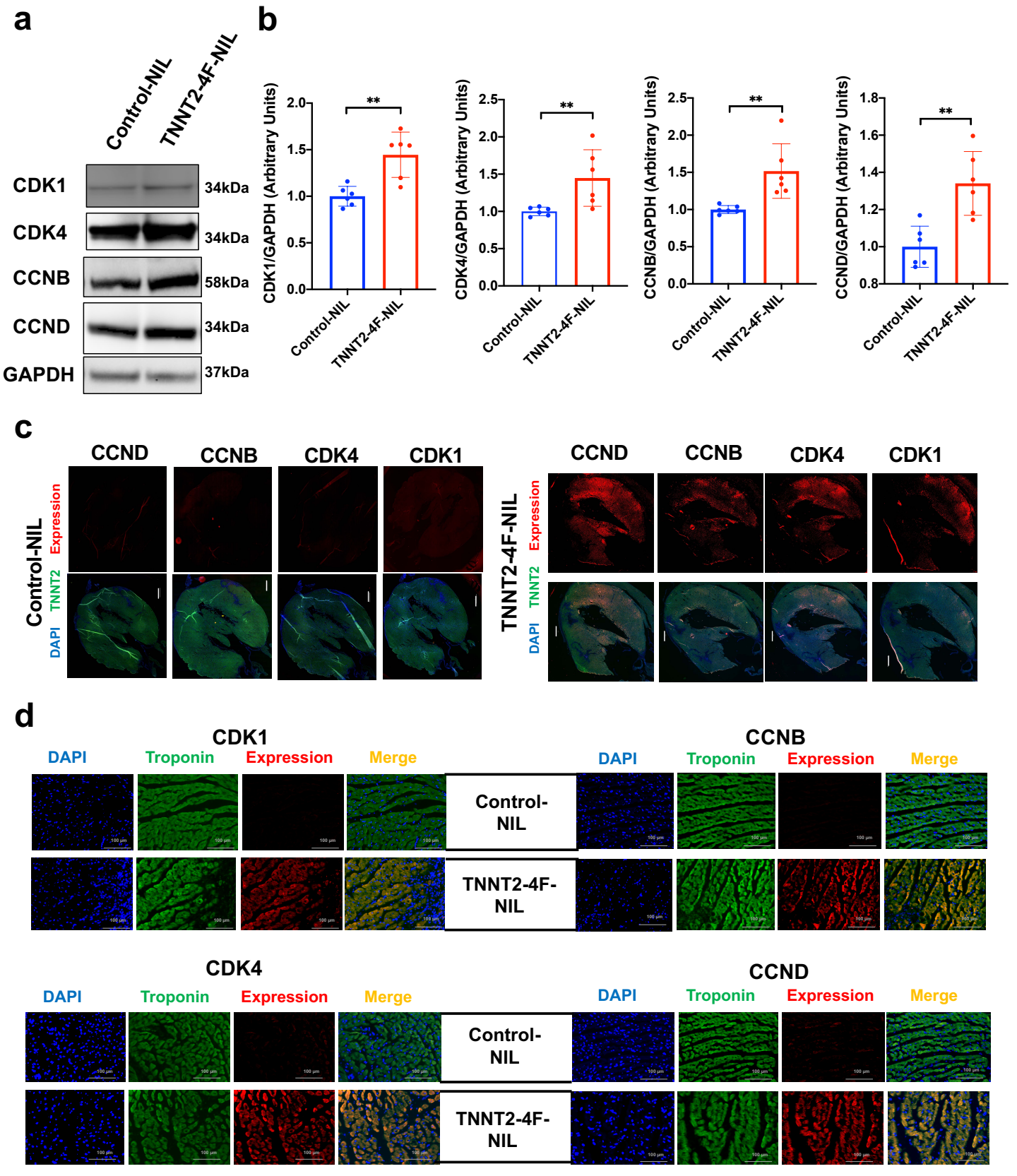

Supplemental Fig. 9. TNNT2-4F-NIL drives significant 4F expression in rat hearts *in vivo* six days post-injection

(a) Representative Western blots from protein lysates of rat heart injected with TNNT2-GFP-NIL (Control-NIL), or TNNT2-4Fpolycistronic-NIL (TNNT2-4F-NIL) and harvested after six days to demonstrate the cell cycle factors' protein expression. **(b)** Quantification of the protein expression of each cell cycle factor (n=3 animals in each group done in duplicates, **p<0.01 compared to the GFP-NIL control group, error bars indicate the S.D.). **(c)** Representative images of the whole section of rat hearts (Scale bar=1mm) or **(d)** zoom-in higher magnification at the injected site (Scale bar=100μm) collected six days following intramyocardial injection of TNNT2-4F-NIL or control NIL and stained for troponin-T (green), DAPI (Blue), and red for CDK1, CDK4, CCNB or CCND.

Supplemental Fig. 10

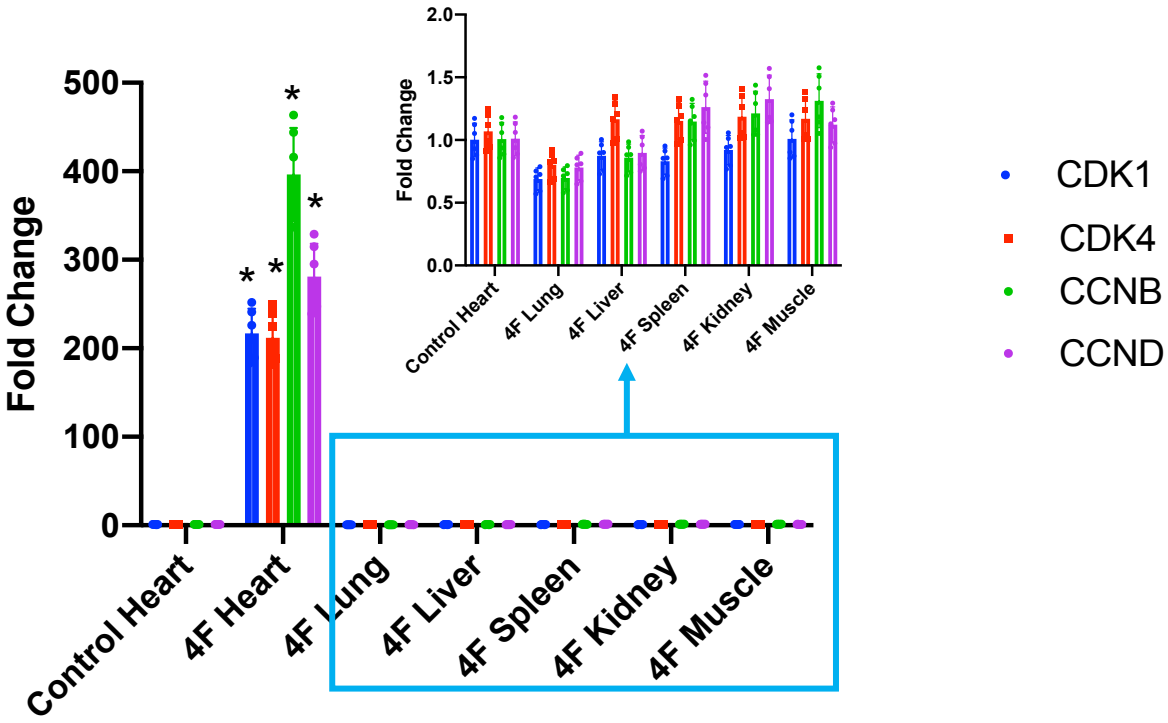

Supplemental Fig. 10. Intramyocardial injection of TNNT2-4F-NIL drives human CDK1, CDK4, CCNB, CCND expression specifically in the rat hearts

Bar graph shows qRT-PCR quantification for human gene expression of the four cell cycle genes in different tissues from rats six days after intramyocardial injection of TNNT2-4F-NIL or control TNNT2-GFP-NIL (n=3 animal per group each in duplicate, *p<0.05 compared to the control group, error bars indicate the S.D.).

Supplemental Fig. 11

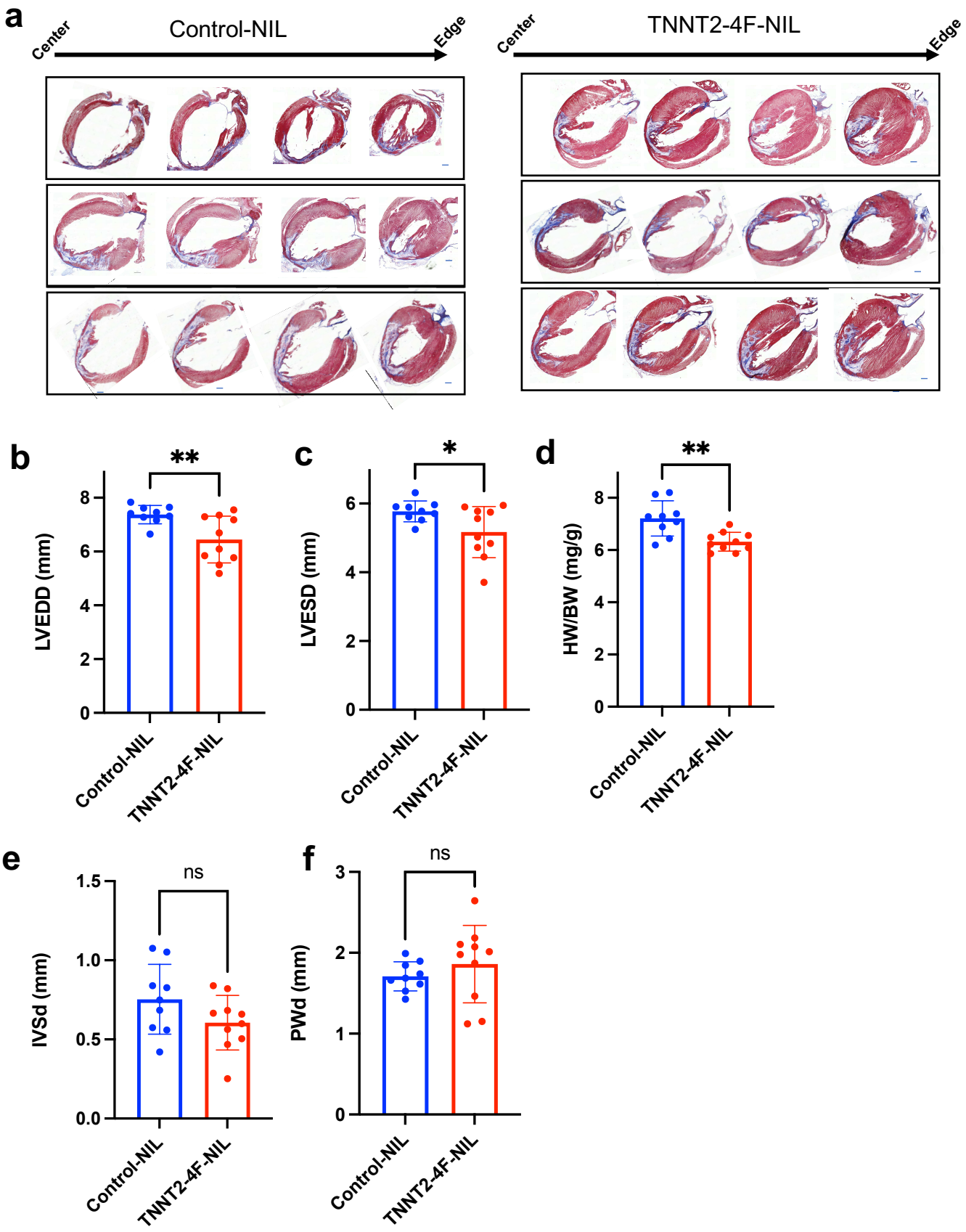

Supplemental Fig. 11. TNNT2-4F-NIL doesn’t induce cardiac hypertrophy.
(a) Representative images of rat hearts stained with Masson's trichrome stain (healthy myocardium stains red and fibrotic tissue stains blue) at the end of the experiment (scale bar=2mm). Column bars show the quantification of left ventricular end diastolic diameter (LVEDD) **(b)**, left ventricular end systolic diameter (LVESD) **(c)**, heart weight/body weight (HW/BW) **(d)**, Interventricular septum thickness at diastole (IVSd) **(e)**, and posterior wall thickness at diastole (PWd) **(f)**. (n=9-10 animals, *$p<0.05$, or **$p<0.01$ compared to Control-NIL group, error bars indicate the S.D.).

Supplemental Fig. 12

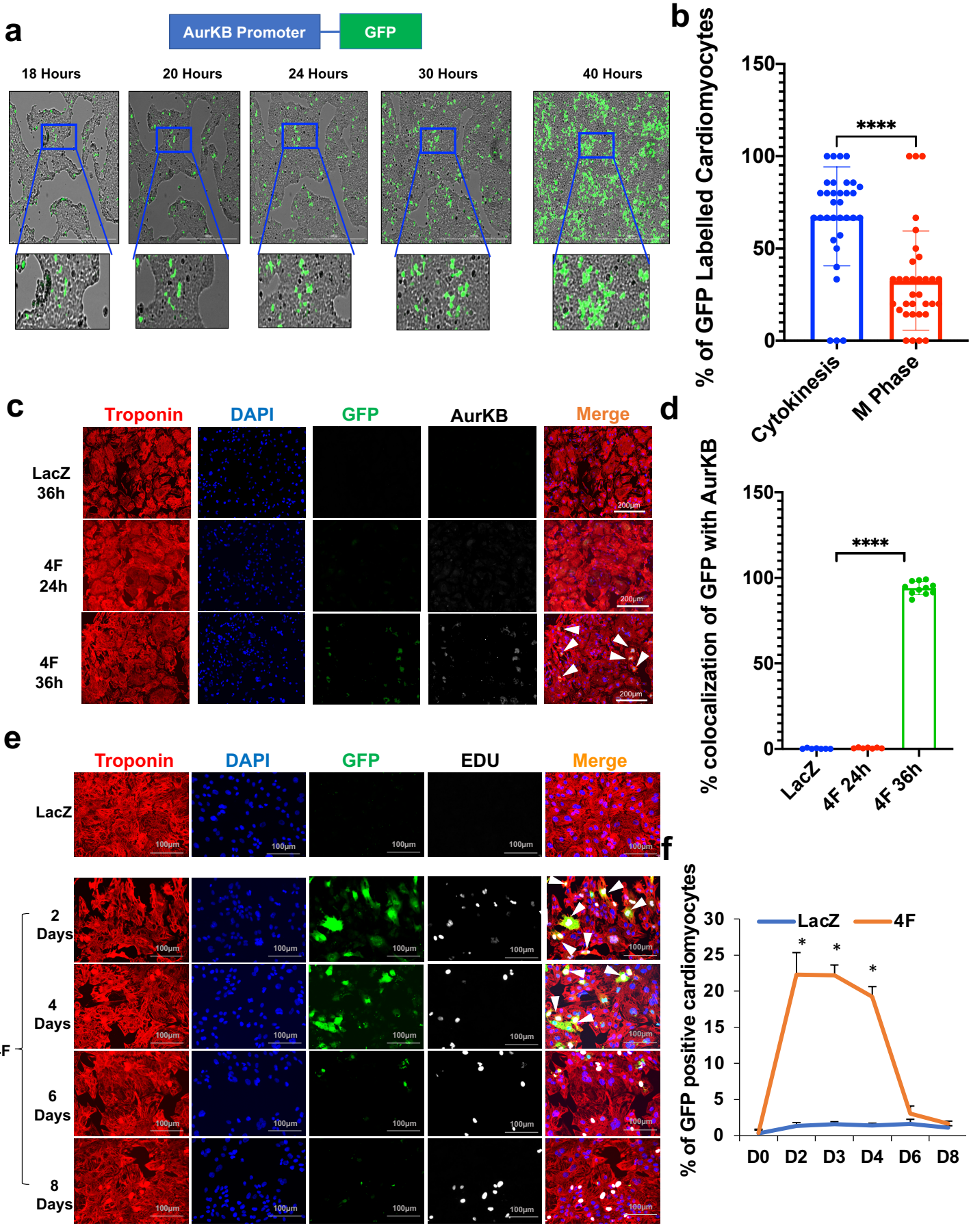

Supplemental Fig. 12. AurKB-GFP is a novel mitosis marker *in vitro*

(a) Schematic diagram of the AurKB-GFP construct and representative live-cell images of HEK293 cells treated with AurKB-GFP-IL (Scale bar=1000μm). **(b)** Quantification of live video images of GFP positive hiPS-CMs that visually completed cytokinesis (200 cells analyzed from in each group from 2 independent experiments, a total of 33 videos analyzed, ****p<0.0001, error bars indicate the S.D.). **(c)** Representative images of hiPS-CMs treated with LacZ or 4F adenovirus and AurKB-GFP-IL for 24, 36 hours and stained with antibody against troponin-T (red), GFP (green), and Aurora kinase B protein (AurKB) (gray) (Scale bar 200μm). **(d)** Quantification of the colocalization of GFP positive cardiomyocytes with the AurKB protein (n=3 independent experiments conducted in triplicate, ****p<0.0001 compared to LacZ, error bars indicate the S.D.). **(e)** Representative images of hiPS-CMs treated with LacZ or 4F adenovirus and AurKB-GFP-IL for 2, 4, 6, and 8 days and stained with antibody against troponin-T (red), GFP (green), and EDU (gray) (Scale bar 100μm). **(f)** Quantification of the percentage of GFP positive cardiomyocytes (n=2 independent experiments conducted in triplicate, *p<0.05 compared to D0).

Supplemental Fig. 13

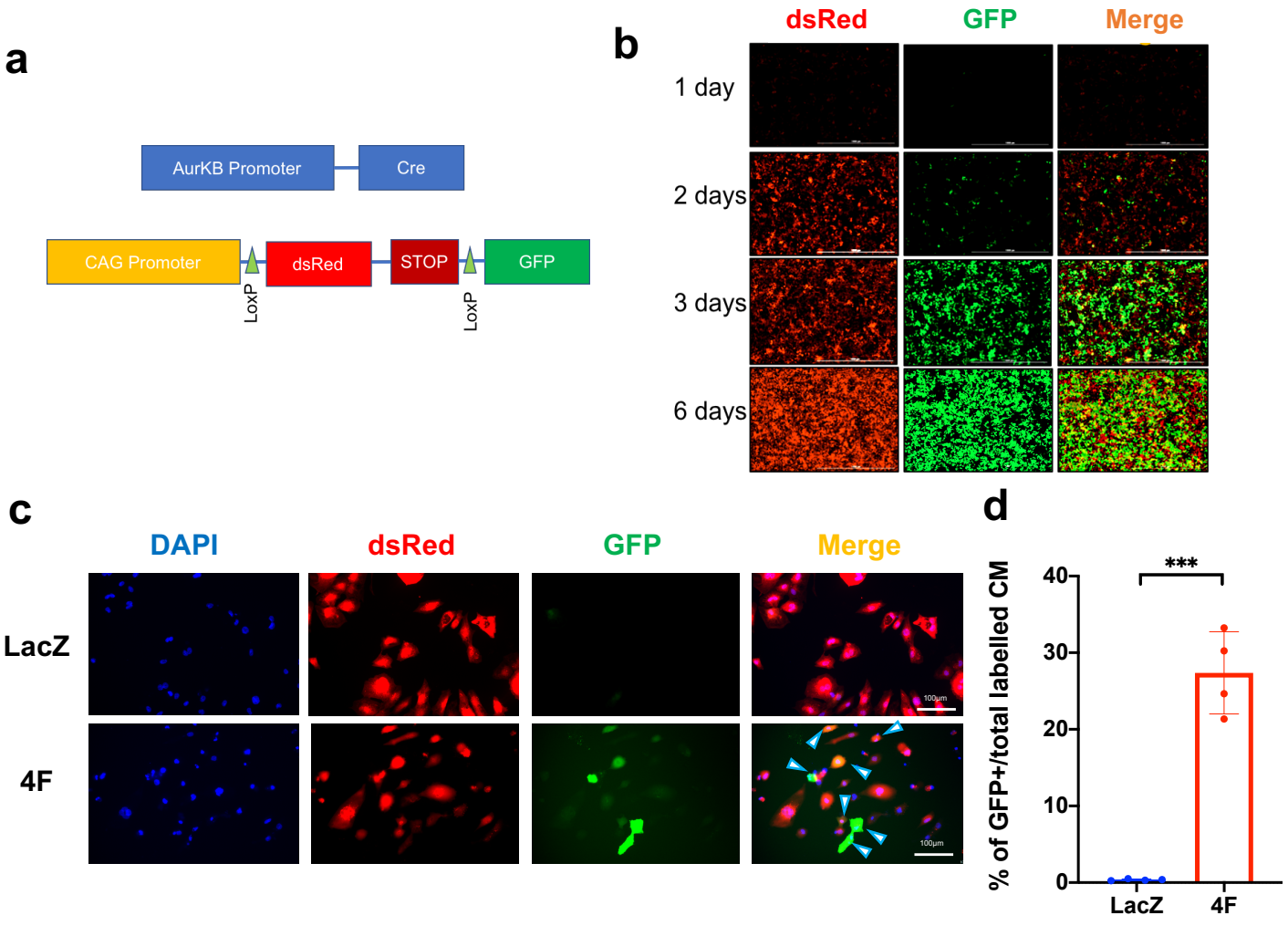

Supplemental Fig. 13. Double reporter system to track mitosis events based on the AurKB promoter

(a) Schematic diagram of the double reporter system vectors design. **(b)** Live images of HEK293 cells treated with the double reporter system over time, showing the switch between red and green color during proliferation (Scale bar=1000μm). **(c)** Representative images of live hiPS-CMs treated with LacZ or 4F adenovirus and the double reporter system for 48 h. Live cell DAPI was added to label the nuclei. Arrows point to cardiomyocytes with color switch following proliferation (Scale bar=100μm). **(d)** Quantification of the percentage of GFP positive cells (n=4 independent experiments each in duplicate, ***p<0.001 vs. LacZ control group, error bars indicate the S.D.).

Supplemental Fig. 14

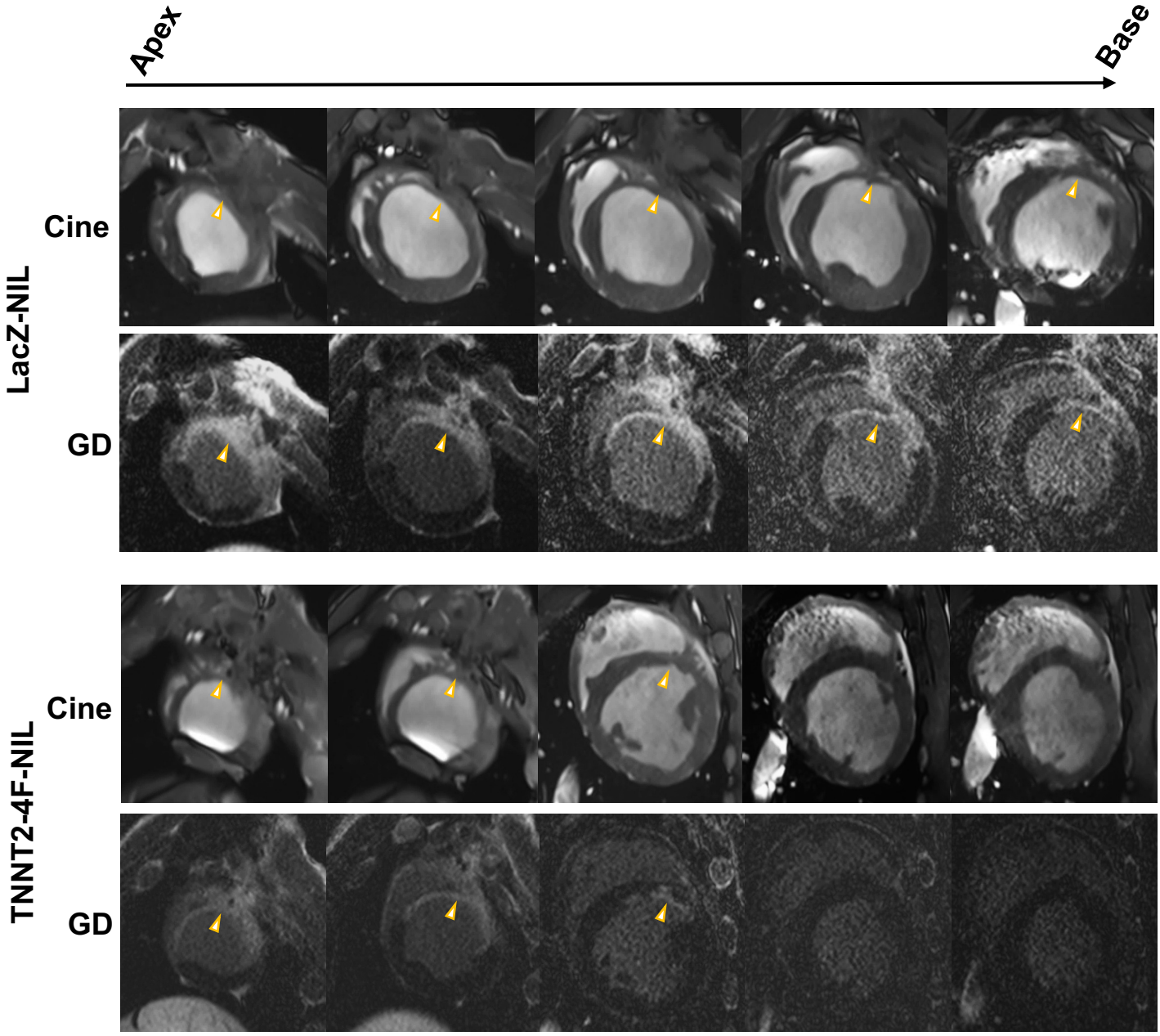

Supplemental Fig. 14. Representative magnetic resonance images of porcine hearts four weeks post-treatment

Representative cross-section magnetic resonance images (MRI) 4 weeks after viral injection before (cine) and after gadolinium enhancement of the scar (GD) shows ventricular wall thinning in cine mode and white scar tissue in GD mode at the infarct site in the control group with significant improvement in animals that received the TNNT2-4F-NIL (arrows). Multiple images from the bottom (apex) to the top of the ventricular chambers (base) are shown.

Supplemental Fig. 15

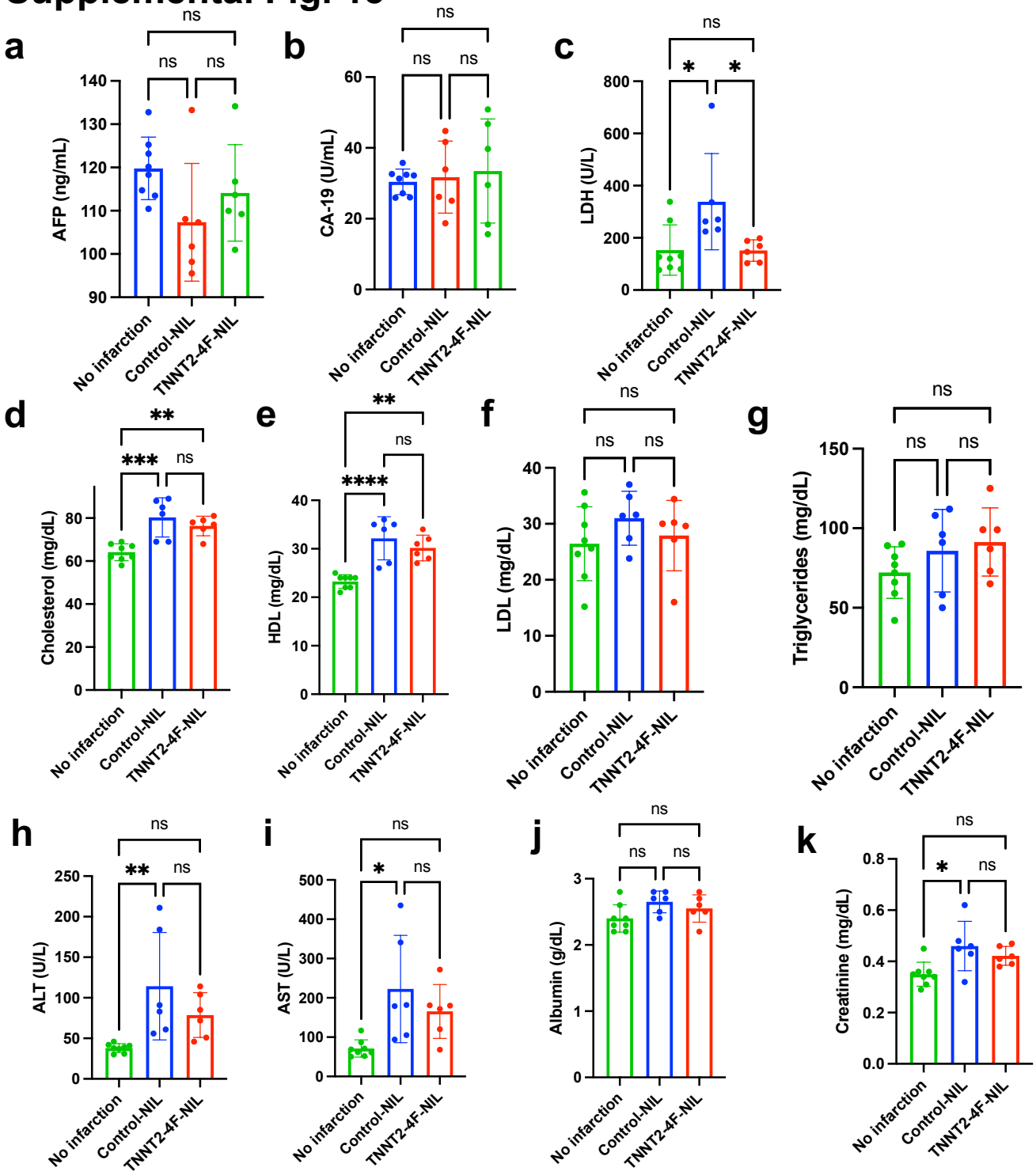

Supplemental Fig. 15. Plasma toxicology profile for rats treated with control or TNNT2-4Fpolycistronic-NIL virus for 16 weeks.
Column bars show the plasma levels of the cancer markers; (Alpha fetoprotein (AFP) **(a)**, and CA-19 **(b)**), the cell damage marker (lactate dehydrogenase (LDH)) **(c),** lipid profile markers (total cholesterol **(d)**, HDL cholesterol **(e)**, LDL cholesterol **(f)**, and Triglyceride **(g)**), Liver function markers (ALT **(h)**, AST **(i)**, and Albumin **(j)**), and kidney function marker (creatinine **(k)**) (n=6-8 animals, *p<0.05, **p<0.01, ***p<0.001, or ****p<0.0001 compared to the other groups, error bars indicate the S.D.).